Studies on structures and properties of TEMPO-oxidized cellulose nanofibril films

（TEMPO 酸化セルロースナノフィブリルフィルムの構造と特性に関する研究）

Hayaka Fukuzumi

福　住　早　花

Department of Biomaterial Sciences

Graduate School of Agricultural and Life Sciences

The University of Tokyo

TABLE OF CONTENTS

CHAPTER 1

General introduction

1.1 Cellulose

1.1.1 Background

Cellulose is the most abundant organic polymers, representing about 1.5×10^{12} tons of the total annual biomass production.[1] It is a structural component in wood, cotton, hemp and other plant-based materials. It is also synthesized by algaes, certain fungi, tunicates, and some bacteria.[2,3] Thousands of years prior to the first discovery of cellulose by Payen in 1838, it has been used in the form of wood, cotton, and other plant fibers as an energy source, building materials, and clothing.[1,4] In the 1920–1940s, cellulose was at the center of the pioneering research on polymers, with the subsequent years being devoted to the industrial application of cellulose derivatives.[5,6] The oil crisis of the 1970s generated considerable interests in the use of cellulose as a source of biomass for the bioproduction of organic chemicals.[5]

At the present day, cellulose is mainly produced from wood and cotton, whose cellulose contents are 40–50% and 90%, respectively, for industrial use. Wood pulp is mainly used to produce paperboards and papers; to a smaller extent it is converted into regenerated and chemically-modified products such as films, fibers, and water-soluble thickners.[1] Recent environmental issues and demands for sustainable resources have driven the fundamental researches and applications of cellulose. Converting cellulose from energy crops into biofuels, such as cellulosic ethanol, is under investigation as an alternative fuel source. Furthermore, utilization of cellulose for high functional materials, such as bio-nanofibers, is also extensively studied as an alternative to petroleum-based materials.

1.1.2 Structure

Figure 1.1 shows the hierarchical structure of wood cellulose. The molecular

structure of cellulose is a carbohydrate polymer generated from repeating β-D-glucopyranose molecules that are covalently linked through glycoside bonds between the equatorial OH group of C4 and the C1 carbon atom (β-1,4-glucan). Cellulose is a linear-chain polymer with a large number of hydroxyl groups (three per anhydroglucose unit). The crystalline state of cellulose is determined by the arrangement of the glucan chains during cellulose biosynthesis.[7] In nature, most celluloses are produced as crystalline polymers defined as cellulose I, whose glucan chains are parallel to each other and packed side by side to form cellulose microfibrils. The microfibril widths may vary depending on their origin. For example, the width of microfibrils is 3–4 nm in most plants, while 20 nm in a certain algae. The biosynthesis[2,7–11] and crystal structure[12–16] of cellulose microfibril were extensively reviewed elsewhere.

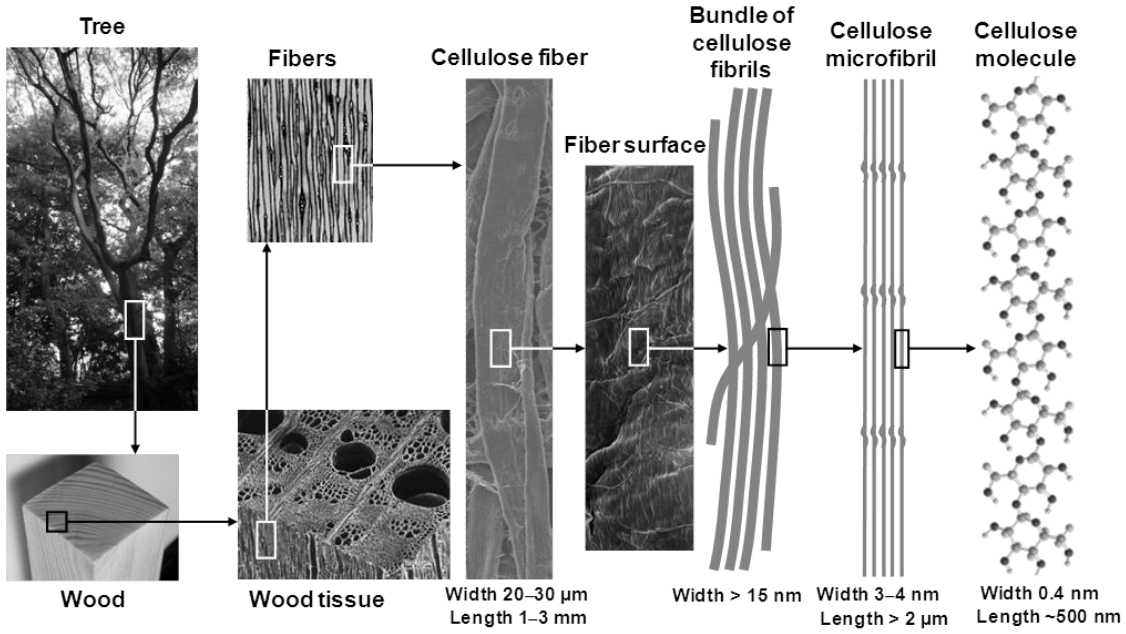

Figure 1.1. Hierarchical structure of wood biomass and the characteristics of cellulose microfibrils.

In plant cellulose, microfibrils form bundles with widths of > 15 nm. The aggregation of microfibrils is dependent on the cell wall type.[17] Several geometrical models were proposed with respect to fibril aggregation in cell walls texture.[18–21]

Cellulose fibers with widths of 20–30 μm are main components in pulp and paper. Cellulose fibers in softwood mainly consist in tracheids, which constitute 90% of principal cells.[22] Trasheids are highly elongated, lignified cells with tapering ends having an average width of about 30 μm and length of 3–5 mm. Hardwoods contain two principal cell types: wood fibers and vessel elements.[22] The wood fibers are elongated, thick-walled fibers having ~20 μm in width and > 1 mm in length. The vessels are relatively large in width and short in length. Wood tissue is composed mixture of cellulose, hemicellulose and lignin.

1.2 Cellulose fibers for pulp and paper

Pulp is the product of the individual fibers in wood or nonwood plants such as bagasse, bamboo, kenaf, wheat, hemp and flax.[22] Pulps are roughly classified into two types according to pulping process; mechanical and chemical pulps. Mechanical pulp is produced by a high-speed rotation of wood bolts or chips in water using a stone grinder or a disk refiner. Mechanical pulp can be obtained in high yields, but it contains a significant amount of lignin. Thermomechanical pulp involves the pre-steaming of raw wood chips at high temperature and pressure to soften the lignin before refining. Chemical pulping is a process to dissolve and remove lignin from wood chips with a pulping reagent; the pulping process is technically called “cooking”. Typical chemical pulps are sulfite and kraft pulps. In sulfite pulping process, cooking liquor is prepared as follows. Sulfur is burned to make sulfur dioxide, which is subsequently dissolved in water. When a base (commonly calcium) is added to the liquor, first bisulfite and then monosulfite is formed. Most of the lignins in wood chips are sulfonated by these chemicals and dissolved in cooking liquor during the sulfite process. A large amount of hemicellulose and a slight amount of cellulose are also dissolved by acid hydrolysis. The sulfite pulp contains cellulose of about 95%, hemicellulose of about 5%, and a small amount of lignin.[23] Since manufactured in 1874, sulfite pulp had been used for papermaking and rayon production because it can be produced in high yields with lower

cost of cooking chemicals, and has high brightness without bleaching. However, the sulfite process has some disadvantages; applicable wood species are limited and papers produced from sulfite pulps are distinctly weaker than those produced from kraft pulp. With the development of efficient kraft recovery and bleaching systems in 1930s–1950s, the kraft process became principal process for producing chemical pulps.

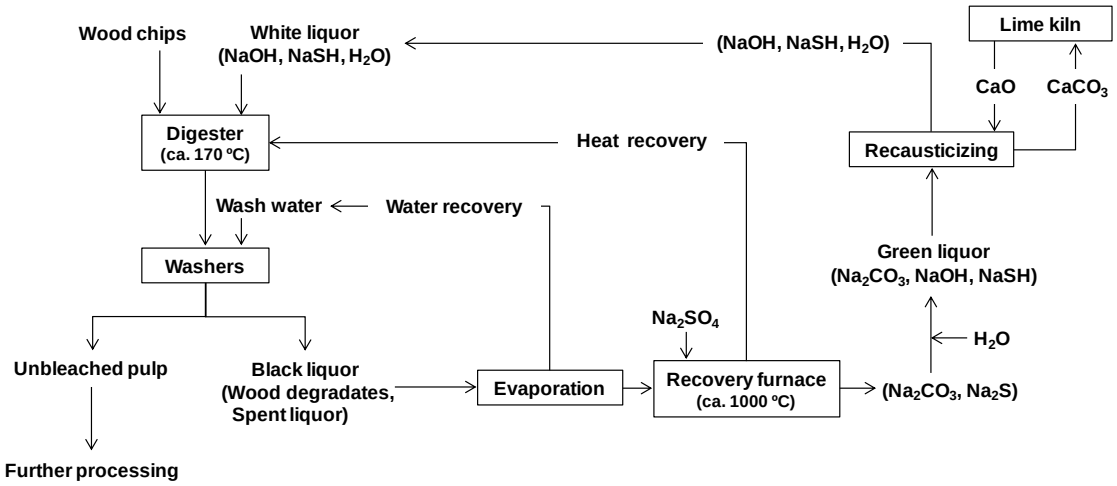

Figure 1.2. Schematic flow diagram of the kraft process.

Kraft process is often termed sulfate process, although the active cooking agent is not sulfate but are sodium hydroxide and sodium hydrosulfide. The schematic flow of kraft process is illustrated in Figure 1.2.[22,23] The cooking liquor is composed of sodium hydroxide and sodium hydrosulfide which are generated from sodium carbonate and sodium sulfide. Wood chips and the white cooking liquor are charged to a digester heated at 150–180 ºC. During this process the cleavage of β-O-4 ether linkage occurs to lignin; alkaline hydrolysis and peeling reaction occur to cellulose and hemicelluloses to some extent.

After the digestion is completed, the cooked chips are washed and separated into unbleached pulp and black liquor. The unbleached pulps with the yield of about 50% are frequently used for paperboard, and otherwise subjected to bleaching process. The black liquor combined with washing water is evaporated, and the concentrated black liquor is then incinerated in a recovery furnace to which sodium sulfate is added for supplying sodium and sulfur. This produces sodium carbonate and sodium sulfide, which is

subsequently hydrolized to generate green liquor. The liquor is then causticized by reaction with slaked lime, after which the precipitated calcium carbonate is removed. The calcium carbonate is then burned to regenerate lime for reuse in the causticization. The advantages of kraft pulping are as follows; 1) any wood species can be applied to this process, 2) the recovery process of cooking chemicals is well established, and 3) the produced pulp has sufficient strength for papers and paperboards.

The name “kraft”, means strength in German and Swedish, has been applied to this process because the produced pulp had higher strength compared with other pulps.[22,24] The kraft pulp contains about 85% cellulose, about 15% hemicellulose, 2–5% residual lignin.[22,23] The residual lignin influences on optical and physical properties of pulps. If a pulp with high brightness is required for printing and writing grades, bleaching process is applied. Almost all bleaching processes now consist of multiple stages containing oxidation and alkali-extraction. Laboratory process of delignification is mostly based on the reaction of moist wood with an acidified solution of sodium chlorite. The prepared cellulose or holocellulose are depolymerized to some extent by the delignification treatment.[22]

1.3 Studies on nano-sized cellulose

The production of nano-sized cellulose fibers and their applications have gained increasing attention due to their high strength and stiffness combined with light weight, biodegradability and renewability.[3] In this section, various approaches to prepare nanocellulosic materials from native plant sources are introduced.

Partially or significantly fibrillated cellulose fibers have been used as beaten pulps and micro-fibrillated celluloses (MFC), respectively. Since developed in 1980s, MFC has been produced from wood pulp at the industrial level by repeated high-pressure homogenization treatment in water,[25,26] and has been used as a filter aid and thickener. Generally, high energy consumption is unavoidable for the nanofibrillation of plant celluloses because it requires partial cleavage of numerous numbers of inter-fibrillar

hydrogen bonds. Wood cellulose fibers have been converted to nanofibrils with width of 20–100 nm by treatment with a grinder.[27–29] Other than wood cellulose fibers, agricultural waste and never-dried wood holocelluloses were studied as resources for the nanofibrillation of cellulose.[30–34]

Chemically-assisted nanofibrillations of various materials, such as wood, cotton, ramie, and bacterial and tunicate celluloses, have been extensively studied at the laboratory level. In most cases, anionically charged functional groups are introduced on cellulose microfibril surfaces to form strong electrostatic repulsion between the microfibrils in water. A traditional and representative method to introduce charged groups onto cellulose microfibril surfaces is acid hydrolysis with 64% H_2SO_4 at 45 ºC for 1–4 h.[35–39] When wood celluloses are subjected to the acid hydrolysis followed by sonication, spindle like cellulose nanocrystals (CNC) or nanowhiskers (CNW) with 5–10 nm width and 50–200 nm length are obtained. However, weight recovery ratios are low as only 30–50%.[36]

Cellulase-pretreatment or partial carboxymethylation of wood celluloses enabled a reduction of energy consumption in nanofibrillation processes using a refiner and high-pressure homogenizer treatments.[40–42] Graft-polymerization of acrylonitrile onto wood celluloses and successive mechanical treatment seems to cause dispersion of partially anionic groups-grafted nanocellulose in water.[43] MFC, enzymatically or chemically modified MFCs, and acid-hydrolyzed CNCs have been studied primarily for applications as fillers in nanocomposites and electro-optical films.[4,44] However, it has been difficult to isolate completely individualized cellulose microfibrils from plant cellulose fibers without serious damage or yield losses, because numerous hydrogen bonds are present between cellulose microfibrils in cellulose fibers. Plant cellulose microfibrils can be regarded as bio-based nanofiber with uniform widths, high crystallinity and high aspect ratios originally present in the plant cell walls (Figure 1.1). In 2006, Isogai's group of the University of Tokyo has developed a new method to prepare completely individualized cellulose nanofibrils 3–4 nm wide and a few microns long from wood cellulose fibers by 2,2,6,6-tetramethylpiperidine-1-oxyl radical

(TEMPO)-mediated oxidation under moderate aqueous conditions.[45–47]

1.4 TEMPO-mediated oxidation of cellulose

TEMPO-mediated oxidation of cellulose at alkaline condition is illustrated in Figure 1.3. TEMPO and its analogues are water-soluble, commercially available and stable nitroxyl radicals. Catalytic oxidation using TEMPO has opened a new field of efficient and selective conversion chemistry of alcoholic hydroxyl groups to aldehydes, ketones and carboxyl groups under mild conditions. Many related studies have been extensively carried out in the last two decades, and have been reviewed in detail.[48,49] Particularly, de Nooy et al. first applied TEMPO-mediated oxidation to water-soluble polysaccharides such as starch, amylodextrin and pullulan for regioselective conversion of C6 primary hydroxyl to carboxylate groups.[50] In this system, catalytic amounts of TEMPO and sodium bromide were dissolved in polysaccharide solutions at pH 10–11, and oxidation was started by the addition of sodium hypochlorite solution as a primary oxidant.[51,52] Various TEMPO-mediated oxidation reactions of mono-, oligo- and polysaccharides for regioselective conversion of primary hydroxyls to carboxylate groups have been reviewed elsewhere.[53,54]

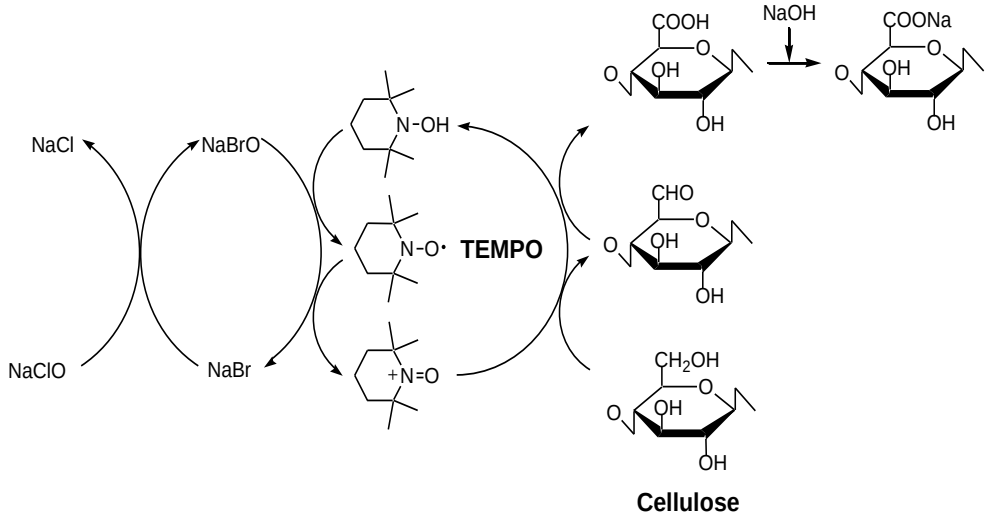

Figure 1.3. Scheme of TEMPO-mediated oxidation of cellulose at alkaline condition.

1.4.1 TEMPO-mediated oxidation of regenerated cellulose

For regenerated and mercerized celluloses, ball-milled or liquid NH_3-treated native celluloses became transparent solutions as the oxidation proceeded; water-soluble oxidized products were obtained in these cases.[55–57] The oxidized products had almost homogeneous chemical structures of sodium (1,4)-β-D-polyglucuronate, which is named as cellouronic acid (CUA). Hence, the C6 primary hydroxyls of celluloses can be entirely and selectively converted to C6 sodium carboxylate groups by TEMPO-mediated oxidation (Figure. 1.3).[55–57] However, drastic depolymerization was unavoidable for CUA prepared by TEMPO oxidation at alkaline condition plausibly owing to β-elimination of C6 aldehyde groups formed as intermediate structures, and/or cleavage of the (1,4)-β-glycoside bonds of CUA by radical species formed in situ as side reactions during TEMPO-mediated oxidation.[58–63] Alternative TEMPO oxidation at neural condition with addition of sodium hypochlorite and sodium chlorite was thus proposed to suppress the intense depolymerization during reaction. The details of this TEMPO-oxidation system were reviewed elsewhere.[64,65] CUAs are both biodegradable and metabolizable, and have relatively low-molecular weights, so they have potential application as new biodegradable polymeric builders in detergents to capture calcium ions in laundry water.[66]

1.4.2 TEMPO-mediated oxidation of native cellulose

When TEMPO-mediated oxidation is applied to native celluloses with the cellulose I crystal structure, such as cotton linters, bleached kraft and sulfite pulps, softwood thermomechanical pulp, bacterial cellulose and ramie fiber, the original fibrous morphologies are unchanged even after the oxidation with sufficient amounts of reagents.[45–47, 66] Every one of two glucosyl residues of the extended cellulose chains present on the crystalline microfibril surfaces can be converted into a sodium glucuronosyl residue by the oxidation under suitable oxidation conditions.[66–68] Thus, TEMPO-mediated oxidation of native cellulose is a type of regioselective surface modification of crystalline native cellulose microfibrils, and allows the formation of

anionic carboxylate groups with quite high densities on the microfibril surfaces. As is the case with regenerated cellulose, significant depolymerization is inevitable for native celluloses during the TEMPO-mediated oxidation at alkaline condition. The alternative TEMPO oxidation system at neutral condition suppressed the depolymerization of the oxidized celluloses to some extent.[47]

When the oxidized cellulose contains sufficient amounts of carboxylate groups on the microfibril surface; for example more than approximately 1.0 mmol g^{-1} for hardwood and softwood bleached kraft pulp, the fibrous oxidized cellulose/water slurries were converted to transparent and viscous nanofibril-dispersions by mechanical disintegration treatment using a household blender, double-cylinder-type homogenizer or ultrasonic homogenizer for 2–10 min.[45–47,66,67] In the case of wood cellulose, the prepared TEMPO-oxidized cellulose nanofibrils are 3–4 nm in width and a few microns in length, which corresponds to microfibril size (Figure 1.1). Additionally, other native celluloses such as cotton linters, ramie, bacterial, tunicate and algal celluloses were also converted to individual nanofibrils, whose widths correspond well to their crystal sizes. The large amounts of anionically charged sodium carboxylate groups present in high densities on the microfibril surfaces may cause the individualization of cellulose microfibrils by electrostatic repulsion and/or osmotic effects in water.[66]

Figure 1.4 shows a schematic model of the preparation of individualized cellulose nanofibrils from wood cellulose such as kraft and sulfite pulps. The model is illustrated in two-dimension for simplicity. These pulps contain 5–15% of disordered hemicelluloses presenting in the spaces between cellulose microfibrils. During the TEMPO-mediated oxidation, the oxidized TEMPO molecules and/or nitrosonium ions can easily penetrate into the sponge-like hemicelluloses regions. Thus, these pulps provide the most efficient production of the TEMPO-oxidized cellulose nanofibrils.[66] The advantageous points of TEMPO-oxidized cellulose nanofibrils are as follows. It is the only method to obtain long and individualized cellulose microfibrils (though the microfibril surfaces are modified). Co-oxidant reagents are inexpensive. The oxidation system is conducted in environmentally-benign conditions (aqueous, pH 10–11, room

temperature, and atmospheric pressure). The surface modification reduces energy consumption in mechanical disintegration process. The preparation method is suitable for production at the industrial level.[66]

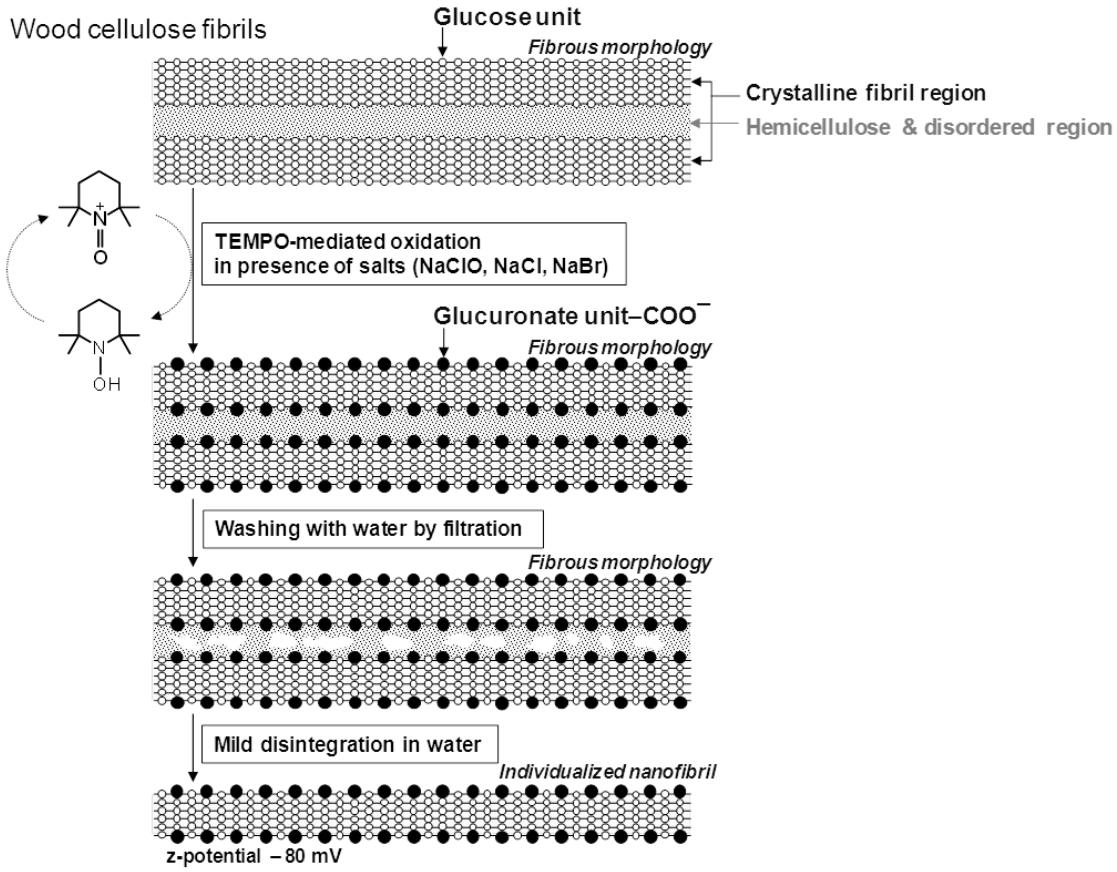

Figure 1.4. Schematic model of the preparation of individualized cellulose nanofibril by TEMPO-mediated oxidation and subsequent disintegration process.

1.5 Objective of this study

The research and development of nanofibers, which defined as nano-sized fibers <100 nm wide or micron-sized fibers with nano-dimension cross sectional structures, have been extensively promoted by both academia and industry in the nanotechnology field. Nanofibers have extremely large surface areas, and the properties are sometimes significantly different from those of the bulk materials. TEMPO-oxidized cellulose nanofibril is a new nanofiber having remarkable advantages in terms of extremely small

diameter, high crystallinity, and bioproductivity, together with environmentally friendly preparation process. Film is one of the important bulk materials to understand fundamental properties of the new cellulose nanofibrils. The objective of this study is to characterize film properties and structures of the new cellulose nanofibrils. Additionally, some of the film properties were improved by surface modification or making nanocomposites with synthetic polymers.

References

1. Klemm,D.; Heublein, B.; Fink, H. P.; Bohn, A. *Angew. Chem. Int. Ed.*, **2005**, 44, 3358–3393.
2. Brett, C. T. *Int. Rev. Cytol.*, **2000**, 199, 161–199.
3. Siró, I.; Plackett, D. *Cellulose*, **2010**, 17, 459–494.
4. Eichhorn, S. J.; Dufresne, A.; Aranguren, M.; Marcovich, N. E.; Capadona, J. R..; Rowan, S. J.; Weder, C.; Thielemans, W.; Roman, M.; Renneckar, S.; Gindl, W.; Veigel, S.; Keckes, J.; Yano, H.; Abe, K.; Nogi, M.; Nakagaito, A. N.; Mangalam, A.; Simonsen, J.; Benight, A. S.; Bismarck, A.; Berglund, L. A.; Peijs, T. *J. Mater. Sci.*, **2010**, 45, 1–33.
5. Nevell, T. P.;Zeronian, S. H. *Ellis Horwood*, *Chichester*, **1985**, pp. 552.
6. Hon, D. N.-S. *Cellulose*, **1994**, 1, 1–25.
7. Saxena, I. M.; Brown, R. M. *Annals of Botany*, **2005**, 96, 9–21.
8. Preston, R. D. *Planta*, **1988**, *174*, 67–74.
9. Delmer, D. P. *Annu. Rev. Plant Physiol. Plant Mol. Biol.*, **1999**. 50, 245–76
10. Cosgrove, D. *J. Nat. Rev. Mol. Cell Biol.*, **2005**, 6, 850-861.
11. Somerville, C. *Annu. Rev. Cell Dev. Biol.*, **2006**, 22, 53–78.
12. Colvin, J. R. *J. Cell. Biol.*, **1963**, 17, 105–109.
13. Hanley, S. J.; Giasson, J.; Revol, J-F.; Gray, D. G. *Polymer*, **1992**, 33, 4639–4642.
14. O'Sullivan, A. C. *Cellulose*, **1997**, 4, 173–207.
15. Wada, M.; Okano, T. *Cellulose*, **1997**, 4, 221–232.

16. Nishiyama, Y.; Langan, P.; Chanzy, H. *J. Am. Chem. Soc.*, **2002**, 124, 9074–9082.
17. Donaldson, L. *Wood Sci. Technol.*, **2007**, 41, 443–460.
18. Fratzl, P. Curr. Opin. *Colloid Interface Sci.*, **2003**, 8, 32–39.
19. Salmén, L. *C.R. Biol.*, **2004**, 327, 873–880.
20. Emons, A. M. C.; Mulder, B. M. *Trends plant sci.*, **2000**, 5, 35–40.
21. Barnett, J. R.; Bonham, V. A. *Biol. Rev.*, **2004**, 79, 461–472.
22. Pulp and Paper Chemistry and Chemical Technology, 3rd ed., Vol. 1, Casey, J. P. Eds., *J. Wilery & Sons*, NY, **1980**. [ISBN 0-471-03175-5]
23. Pulp and Paper Manufacture. The Pulping of Wood, Vol. 1, Macdonald, R. G.; Franklin, J. N. Eds., *McGraw-Hill*, NY, **1969**. [OCLC 85959968]
24. Kleppe, P. J. *Tappi J.*, **1970**, 53, 35–47.
25. Herrick, F. W.; Casebier, R. L.; Hamilton, J. K.; Sandberg, K. R. *J. Appl. Polym. Sci., Appl. Polym. Symp.*, **1983**, 37, 797–813.
26. Turbak, A. F.; Snyder, F. W.; Sandberg, K. R. *J. Appl. Polym. Sci., Appl. Polym. Symp.*, **1983**, 37, 815–827.
27. Taniguchi, T.; Okamura, K. *Polym. Int.*, **1998**, 47, 291–294.
28. Iwamoto, S.; Nakagaito, A. N.; Yano, H.; Nogi, M. *Appl. Phys. A: Mater. Sci. Process.*, **2005**, 81, 1109–1112.
29. Iwamoto, S.; Nakagaito, A. N.; Yano, H. *Appl. Phys. A: Mater. Sci. Process.*, **2007**, 89, 461–466.
30. Dinand, E.; Chanzy, H.; Vignon, M. R. *Cellulose*, **1996**, 3, 183–188.
31. Dinand, E.; Chanzy, H.; Vignon, M. R. *Food Hydrocolloids*, **1999**, 13, 275–283.
32. Hult, E.-L.; Iversen, T.; Sugiyama, J. *Cellulose*, **2003**, 10, 103–110.
33. Abe, K.; Iwamoto, S.; Yano, H. *Biomacromolecules*, **2007**, 8, 3276–3278.
34. Iwamoto, S.; Abe K.; Yano, H. *Biomacromolecules*, **2008**, 9, 1022–1026.
35. Marchessault, R. H.; Morehead and, F. F.; Walter, N. M. *Nature*, **1959**, 184, 632–633.
36. Dong, X. M.; Revol, J.-F.; Gray, D. G. *Cellulose*, **1998**, 5, 19–32.
37. Beck-Candanedo, S. ; Roman and, M.; Gray, D. G. *Biomacromolecules*, **2005**, 6,

1048–1054.

38. van den Berg, O.; Capadona, J. R.; Weder, C. *Biomacromolecules*, **2007**, 8, 1353–1357.
39. Elazzouzi-Hafraoui, S.; Nishiyama, Y.; Putaux, J.-L.; Heux, L.; Dubreuil, F.; Rochas, C. *Biomacromolecules*, **2008**, 9, 57–65.
40. Pääkkö, M.; Ankerfors, M.; Kosonen, H.; Nykänen, A.; Ahola, S.; Österberg, M.; Ruokolainen, J.; Laine, J.; Larsson, P. T.; Ikkala, O.; Lindström, T. *Biomacromolecules*, **2007**, 8, 1934–1941.
41. Henriksson, M.; Henriksson, G.; Berglund, L. A.; Lindström, T. *Eur. Polym. J.*, **2007**, 43, 3434–3441.
42. Wågberg, L.; Decher, G.; Norgren, M.; Lindström, T.; Ankerfors, M.; Axnäs, K. *Langmuir*, **2008**, 24, 784–795.
43. Lepoutre, P.; Hui, S. H.; Robertson, A. A. *J. Macromol. Sci., Part A: Pure Appl. Chem.*, **1976**, A10, 681–693.
44. Habibi, Y.; A Lucia L.; Rojas, O. J. *Chem. Rev.*, **2010**, 110, 3479–3500.
45. Saito, T.; Nishiyama, Y.; Putaux, J.-L.; Vignon, M.; Isogai, A. *Biomacromolecules*, **2006**, 7, 1687–1691.
46. Saito, T.; Kimura, S.; Nishiyama, Y.; Isogai, A. *Biomacromolecules*, **2007**, 8, 2485–2491.
47. Saito, T.; Hirota, M.; Tamura, N.; Kimura, S.; Fukuzumi, H.; Heux, L.; Isogai, A. *Biomacromolecules*, **2009**, 10, 1992–1996.
48. Adam, W.; Saha-Möller, C. R.; Ganeshpure, P. A. *Chem. Rev.*, **2001**, 101, 3499–3547.
49. de Nooy, A. E. J.; Besemer, A. C.; van Bekkum, H. *Synthesis*, **1996**, 10, 1153–1174.
50. de Nooy, A. E. J.; Besemer, A. C.; van Bekkum, H. *Carbohydr. Res.*, **1995**, 269, 89–98.
51. Bailey, W. F.; Bobbitt, J. M.; Wiberg, K. B. *J. Org. Chem.*, **2007**, 72, 4504–4509.
52. Goldstein, S.; Samuni, A. *J. Phys. Chem. A*, **2007**, 111, 1066–1072.
53. de Nooy, A. E. J.; Besemer, A. C.; van Bekkum, H. *Tetrahedron*, **1995**, 51,

8023–8032.

54. Bragd, P. L.; van Bekkum, H.; Besemer, A. C. *Top. Catal.*, **2004**, 27, 49–66.
55. Isogai, A.; Kato, Y. *Cellulose*, **1998**, 4, 153–164.
56. Isogai, T.; Yanagisawa, M.; Isogai, A. *Cellulose*, **2009**, 16, 117–127.
57. da Silva Perez, D.; Montanari, S.; Vignon, M. R. *Biomacromolecules*, **2003**, 4, 1417–1425.
58. Isogai, T.; Saito, T.; Isogai, A. *Biomacromolecules*, **2010**, 11, 1593–1599.
59. Shibata, I.; Yanagisawa, M.; Saito, T.; Isogai, A. *Cellulose*, **2006**, 13, 73–80.
60. de Nooy, A. E. J.; Besemer, A. C.; van Bekkum, H.; van Dijk, J. A. P. P.; Smit, J. A. M. *Macromolecules*, **1996**, 29, 6541–6547.
61. Potthast, A.; Rosenau, T.; Kosma, P. *Adv. Polym. Sci.*, **2006**, 205, 1–48.
62. Potthast, A.; Schiehser, S.; Rosenau, T.; Kostic, M. *Holzforschung*, **2009**, 63, 12–17.
63. Shibata, I.; Isogai, A. *Cellulose*, **2003**, 10, 151–158.
64. Zhao, M.; Li, J.; Mano, E.; Song, Z.; Tschaen, D. M.; Grabowski, E. J. J.; Reider, P. J. J. *J. Org. Chem.*, **1999**, 64, 2564–2566.
65. Hirota, M.; Tamura, N.; Saito, T.; Isogai, A. *Carbohydr. Polym.*, **2009**, 78, 330–335.
66. Isogai, A.; Saito, T.; Fukuzumi, H. *Nanoscale*, **2010**, 3, 71–85.
67. Okita, Y.; Saito, T.; Isogai, A. *Biomacromolecules*, **2010**, 11, 1696−1700.
68. Hirota, M.; Furihata, K.; Saito, T.; Kawada, T.; Isogai, A. *Angew. Chem., Int. Ed.*, **2010**, 49, 7670−7672.

CHAPTER 2

Preparation and characterization of TEMPO-oxidized cellulose nanofibril films and composites

2.1 Introduction

A new cellulose-based nanofibril can be prepared from native celluloses by TEMPO-mediated oxidation under aqueous conditions at room temperature and pH 10. Transparent dispersions can be obtained within several minutes by gentle agitation of the wood TEMPO-oxidized cellulose fiber/water slurries using a blender-type or ultrasonic homogenizer. Transmission electron microscopy (TEM) observations revealed that the gels consisted of individual cellulose nanofibrils with almost uniform widths of 3–4 nm and lengths greater than 200 nm, so that their aspect ratios were higher than 50.[1–3] In this chapter, films of TEMPO-oxidized cellulose nanofibrils (TOCNs) and TOCN-based composites were prepared by casting or filtration of the TOCNs/water dispersions. Extensive characterization of the new TOCN films revealed that the films have unique properties with potential applications for some high-tech materials.

2.2 Experimental section

2.2.1 Materials

Never-dried softwood and hardwood bleached kraft pulp fibers were used as the cellulose sources for TEMPO-mediated oxidation. The pulps contained approximately 90% cellulose and 10% hemicelluloses. Laboratory grade TEMPO, sodium bromide, and 12% sodium hypochlorite solution (Wako Pure Chemicals, Co. Ltd., Japan) were used as received. Poly(vinyl alcohol) (Wako Pure Chemicals, Co. Ltd., Japan) was dissolved in water to prepare a 1% (g/L) solution. Commercial cellophane film (thickness 38 μm), poly(lactic acid) (PLA, thickness 25 μm), poly(ethylene

terephthalate) (PET, thickness 50 μm), low density poly(ethylene) (LDPE, thickness 50 μm), and oriented poly(propylene) (OPP, thickness 50 μm) films were used as received. A cationic papermaking grade alkylketene dimer (AKD) dispersion (AS-202, 12% AKD content, Seiko PMC Co., Japan) was diluted by 0.05%

2.2.2 TEMPO-mediated oxidation

TEMPO-mediated oxidation was applied to a 1% (g/L) cellulose fiber/water slurry with NaClO, catalytic amounts of TEMPO, and NaBr using the previously reported method.[1,2] The cellulose (1 g) was suspended in water (100 mL) containing TEMPO (0.016 g, 0.1 mmol) and NaBr (0.1 g, 1 mmol). The NaClO solution (3.1 g, 5.0 mmol) was added to the slurry, and the mixture was stirred at room temperature and pH 10 until no more 0.5 M NaOH consumption was observed. The TEMPO-oxidized celluloses thus prepared from both softwood and hardwood celluloses had carboxyl and aldehyde contents of 1.5 and 0.3 mmol g^{-1}, respectively.[1-4] 1 out of every 1.7 glucose units in the surface of cellulose microfibrils was oxidized to the glucuronate unit.

2.2.3 Preparation of TEMPO-oxidized cellulose nanofibril (TOCN) films

A 0.1% (g/L) slurry of TEMPO-oxidized cellulose fibers in water (50 mL) was agitated at 15000 rpm for 2 min using a blender-type homogenizer (Excel Auto ED-4, Nissei, Japan) at room temperature. The obtained gel-like dispersion was then sonicated for 6 min using an ultrasonic homogenizer at 19.5 kHz and 300 W output power (7 mm probe tip diameter, US-300T, Nissei, Japan). Unfibrillated and partly-fibrillated fiber bundles were removed from the gel by filtration through a nylon cloth with 20 μm pores. The recovery of TOCN after filtration was >80%. The approximately 0.1% (g/L) TOCN/water dispersion was converted to a hydrogel on a polytetrafluoroethylene (PTFE) membrane with 0.1 μm pore size (Advantec Toyo, Japan) by suction filtration. The TOCN hydrogel was dried in a ventilated oven at 50 °C overnight without forced air-flow. A TOCN film about 20 μm thick was then obtained. Some TOCN films were prepared by casting the dispersion onto a Petri dish and drying at 40 °C for 3 days. The

TOCN cast films with about 10 μm thickness were easily detached from the dish after drying.

2.2.4 Preparation of TOCN composites

20% TOCN/PVA composite film was prepared by the following method. 0.2% TOCN/water dispersion was blended to 1% poly(vinil alcohol) (PVA) aq. The weight ratio of TOCN and PVA was 2:8. The blend solution was agitated at 1500 rpm for 1 day, cast on a plate and dried at 50 ºC for 1 day. Original PVA cast film was prepared by the same procedure as the composite.

A polylactic acid (PLA) film surface-coated with TOCN was prepared by bar-coating of TOCN water dispersion on a corona-treated PLA film. The TOCN layer adhered to the PLA film by air drying without any delamination.

Some of the TOCN cast films were soaked in a 0.05% AKD dispersion for 10 s followed by rinsing thoroughly with water. The wet films were dried at room temperature, and then heated at 100 °C for 10 min.

2.2.5 Analysis

Surface images of the TOCN films were obtained using an atomic force microscopy (AFM) apparatus in tapping mode (SPI 3800N using SI-DF20 Si cantilever, Seiko Instruments Inc., Japan). The film surfaces were also observed with an ultra-high resolution field emission scanning electron microscopy (SEM, Hitachi S-4800) after osmium sputtering at 7 mA for 10 s.

The thermal decomposition behavior was recorded in a nitrogen atmosphere using a thermo-gravimetric analyzer (Ulvac, TGD-9600, Japan) at 10 °C min^{-1}. Thermal expansivity was measured with a Shimadzu TMA-60 instrument at 0.03 N load in a nitrogen atmosphere from 28 to 102 °C at 5 °C min^{-1} after predrying samples at 120 °C for 10 min.

Light transmittance was measured from 200 to 1000 nm wavelength using a Shimadzu UV-1700 UV-vis spectrometer, and correlated based on the film thicknesses

using the Lambert-Beer's law.

Contact angles of 2 μL water droplets were measured at 23 °C and 50% relative humidity (R.H.) using a FAMAS DM500 apparatus (Kyowa Interface Science Co. Ltd., Japan).

Moisture contents were calculated from weight loss of the films after heating at 105 °C for 3 h. Tensile strengths and Young's moduli of the film with 3 mm width and 20 mm length were measured at 1.0 mm min^{-1} and 10 mm span length using a Shimadzu EZ-TEST instrument equipped with a 500 N load cell.

The TOCN/water dispersion was cast on a plasma-treated PLA film with 25 μm thickness to make a TOCN coated layer with 0.8 μm thickness on the PLA film. The TOCN/PLA film was subjected to measurement of oxygen transmission rates (OTRs) using a Mocon ML & SL (Modern Controls Inc., U.S.A.) apparatus under dry conditions according to ASTM 3985 Standard. Water vapor transmission rates (WVTRs) of TOCN cast films were measured using a Mocon PERMATRAN-W 1/50 apparatus according to ASTM 398 Standard. The cell in detector side was set at 10% R.H., and the other side was varied from 40 to 100% R.H. WVTR of each sample was measured for at least 1 h until it reached a stable value.

2.3 Results and discussion

2.3.1 Surface observation

The AFM image in Figure 2.1 shows that the surface of TOCN films consists of randomly assembled nanofibrils. Nanofibril widths were estimated to be 3–4 nm from the height of AFM images, which is in good agreement with TEM measurements.[1,2] When the film surface was observed with SEM after osmium sputtering, fibrous structures about 15 nm in width were observed (Figure 2.1). It is probable that the nanofibrils on the film surface were covered with relatively thick osmium layers by the sputtering process, which is necessary to be able to observe such nanosized organic materials by SEM. From the SEM image, randomly assembled nanofibrils were

observed in the film surface, while the cross-section of the film was composed of densely accumulated nanofibril layers. The orientation of cellulose nanofibrils in a TOCN cast film was evaluated using wide-angle X-ray diffraction.[5] The diagram of the cast film showed ring patterns, indicating a random orientation of the cellulose nanofibrils on the horizontal plane of the film. The diffractogram clearly showed three reflections assigned to the cellulose I crystal structure. In addition, recent TEM observation revealed that domains of uniaxially aligned nanofibrils with different orientation angles formed layers that were nearly parallel to the film surface, as plywood-like hierarchical structures (like a cholesteric liquid-crystal assembly) in plant cell walls.[6] The structure is formed by consolidation of the nanofibril alignment in aqueous dispersions during drying process.

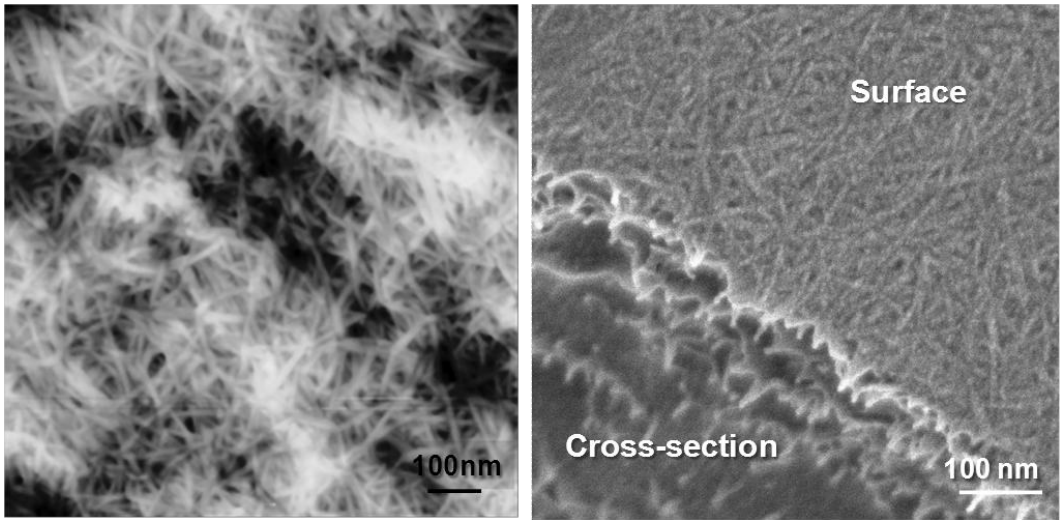

Figure 2.1. AFM (left) and SEM (right) images of the surface of nanofibril films prepared from TEMPO-oxidized softwood cellulose.

2.3.2 Optical properties

Figure 2.2 shows the UV-vis transmittance of approximately 20 μm thick TOCN films prepared from TEMPO-oxidized softwood and hardwood celluloses. The TOCN film obtained was transparent and flexible (photo-graph, Figure 2.2). The transmittance at 600 nm was about 90% for the film prepared from softwood cellulose, while it was about 78% for the film prepared from hardwood cellulose. The softwood TOCN film

had transparency close to cellophane whose transmittance at 600 nm was 94%. The transmittance of the films may relate to dispersibility of nanofibrils in water. The transmittance at 600 nm was about 72% for the TOCN water dispersion prepared from softwood (containing unfibrillated fiber bundles), while it was about 68% for the TOCN water dispersion prepared from hardwood. It indicates that the hardwood TOCN/water dispersion contains larger particles extensively causing light scattering. The difference in transmittance may be explained by the 10% hemicelluloses in the cellulose samples. The hardwood cellulose contains xylan as the predominant hemicellulose which has no C6 primary hydroxyls. On the other hand, the softwood cellulose contains glucomannan whose C6 primary hydroxyls can be converted to sodium carboxylate groups by the TEMPO-mediated oxidation. Syverud et al. reported that *Eucalyptus* (hardwood) kraft pulp had a larger fraction of xylose compared to *Pinus radiata* (softwood) kraft pulp, and xylose content was almost unchanged before and after the TEMPO-mediated oxidation.[7] The presence of xylan molecules in the TEMPO-oxidized hardwood cellulose fibers may interfere with complete dispersion of the TOCNs in water.

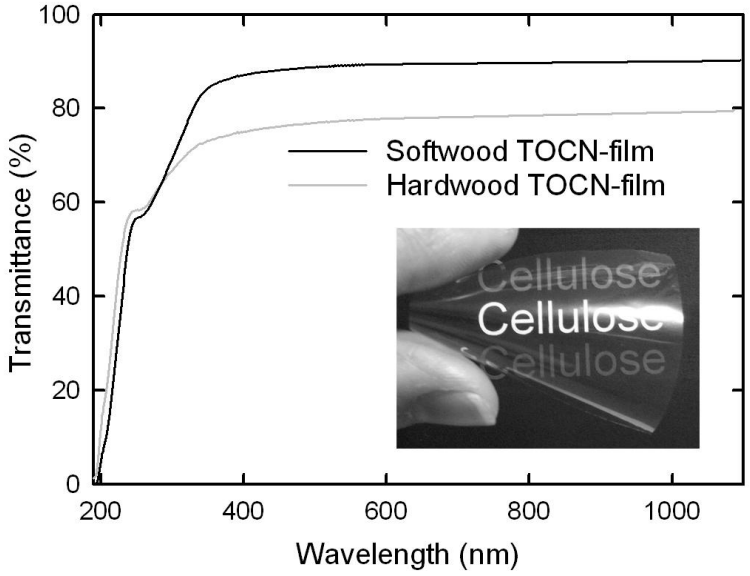

Figure 2.2. UV-vis transmittance of nanofibril films prepared from TEMPO-oxidized softwood and hardwood celluloses. The photograph shows light transmittance behavior of the nanofibril film prepared from TEMPO-oxidized softwood cellulose.

The absorption band shoulder at about 250 nm is caused by C6 aldehyde groups formed as intermediate structures during TEMPO-mediated oxidation of the C6 primary hydroxyls. Aldehyde contents of TEMPO-oxidized wood celluloses are generally lower than 0.3 mmol g^{-1}.[3,4] The absorption at around 250 nm disappeared after reduction of the TEMPO-oxidized celluloses with sodium borohydride or oxidation with sodium chlorite.

The refractive index of the TOCN film was 1.545 ± 0.002 at room temperature, and this value is consistent with those previously reported for cellulose (1.618 along the fiber and 1.544 in the transverse direction).[8]

2.3.3 Thermal properties

Thermal degradation of the TOCN films started at about 200 °C in a nitrogen atmosphere (Figure 2.3), and there was no significant difference between hardwood and softwood. On the other hand, for the original celluloses, degradation began at 300 °C. Thus, the formation of sodium carboxylate groups from the C6 primary hydroxyls of cellulose microfibril surfaces by the TEMPO-mediated oxidation leads to a significant decrease in thermal degradation point. The initial decreases in weight observed at about 60–100 °C for both of the two samples are probably the result of the loss of residual moisture from the samples, because the degrees of weight loss for both the TOCN film and the original cellulose roughly corresponded to their moisture contents.

The thermal expansivity of the TOCN films was measured in a nitrogen atmosphere after heating the film at 120 °C for 10 min to remove the residual moisture (Figure 2.4). The coefficient of thermal expansion (CTE) of the TOCN films was about 2.7 × 10^{-6} °C^{-1}, which is much lower than that of glass (about 9 × 10^{-6} °C^{-1}). The extremely low CTE is possibly caused by the high crystallinity of the nanofibrils and also rigid network structures comprising the TOCN film. The thermal dimension stability of TOCN film as well as high visible light-transparency without the presence of any coexisting polymers is highly advantageous for flexible display panels and electronic devices.

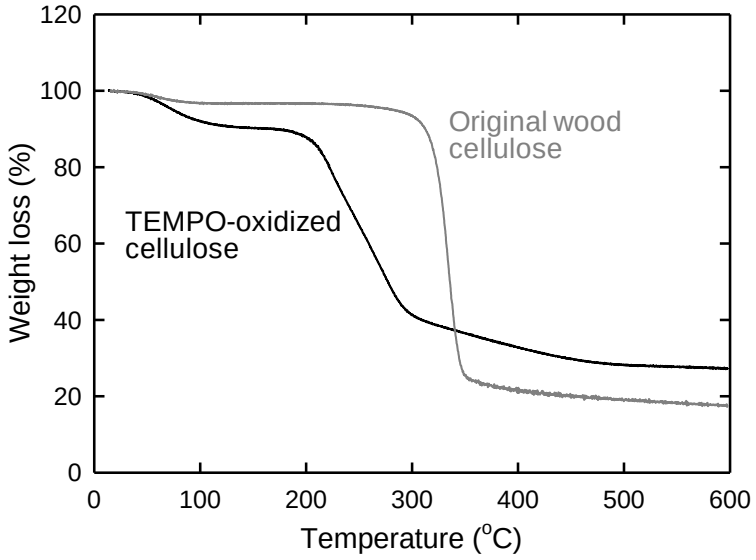

Figure 2.3. Thermogravimetric curves of the original and TEMPO-oxidized celluloses measured in a nitrogen atmosphere.

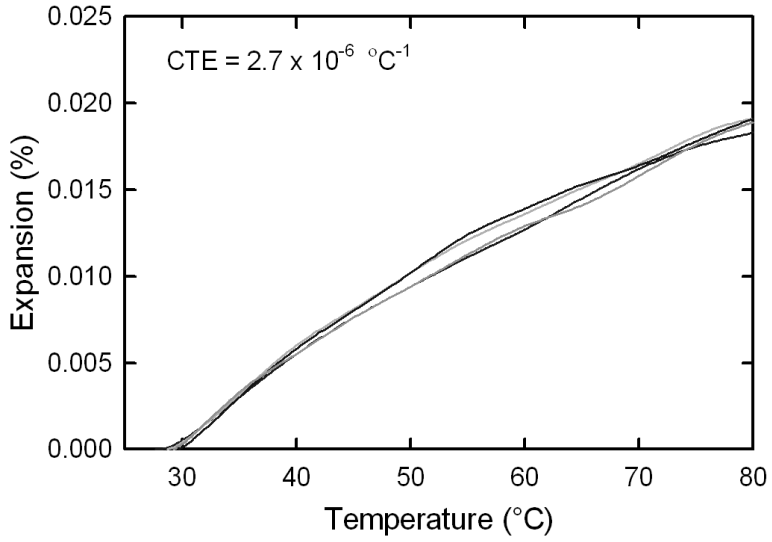

Figure 2.4. Thermal expansion behavior of nanofibril film prepared from TEMPO-oxidized softwood cellulose obtained in a dry nitrogen atmosphere after drying at 120 ºC for 30 min. Four different specimens were measured, and the data were shown as different lines. The coefficient of thermal expansion (CTE) of the TOCN films was about 2.7×10^{-6} °C^{-1}.

2.3.4 Mechanical properties and reinforcing effect in composites

The densities, moisture contents, and tensile properties of the TOCN films prepared from the softwood and hardwood celluloses are listed in Table 2.1. Comparison of tensile strength and elastic moduli between TOCN films with hand-made papers and commercial cellophanes was shown in Figure 2.5. Unlike transparency, no significant difference was observed in tensile properties between softwood and hardwood TOCN films. This result indicates that tensile properties may be more closely related to the film density than dispersibility of nanofibrils in water. Tensile strengths and elastic moduli of the TOCN films were ten and four times, respectively, larger than for papers, which have much smaller densities (Figure 2.5). The densities and moisture contents of the TOCN films were about 1.45 g cm^{-3} and 14%, respectively, which are quite similar to those of commercial cellophane film. This implies that the structure of TOCN film does not resemble to those of papers but is close to those of polymer films. However, the tensile strengths and elastic moduli of the TOCN films were more than twice and sixth times, respectively, larger than for the cellophane film (Figure 2.5). The high crystallinity (ca. 75%) and the high aspect ratios of the nanofibrils were likely to result in such high strength of the TOCN films. Figure 2.5 also shows the reinforcing effect of TOCNs. Both the tensile strength and elastic modulus of the poly(vinyl alcohol) (PVA) film were remarkably improved by 20% TOCN addition. However, similar results would be expected by the addition of only a few % TOCN to PVA if each TOCN is present individually in the TOCN/PVA composite film, because an anisotropic reinforcing filler, such as clay, shows a high level of the nano-reinforcing ability by addition of a few % to a matrix.[9] Therefore, homogeneous distribution of individualized TOCNs without any aggregation in PVA is required to obtain TOCN/PVA composites having the highest reinforcing effect with a minimum addition level.

In this study, carboxyl groups in the TOCN surfaces have the structure of sodium carboxylate groups (TOCN-COONa). TOCN-COONa is easily converted into free carboxyl group (TOCN-COOH) by addition of a dilute hydrochloric acid to the TOCN/water dispersions. A TOCN-COOH/hydrogel is then obtained, and it can be

re-dispersed into a TOCN-COOH/water dispersion at pH 4.6 by sonication.[10] Films prepared from the TOCN-COOH/water dispersions had lower moisture contents, higher Young's moduli and lower elongation at break than those of the TOCN-COONa films, because free carboxyl groups in the TOCN-COOH films can form intra- and inter-nanofibril hydrogen bonds. The lower moisture content of the TOCN-COOH films may also result in the higher Young's modulus and lower elongation at break; the less hydrophilic nature of free carboxyl groups forming hydrogen bonds than that of sodium carboxylate groups.

Table 2.1. Tensile properties of nanofibril films prepared from TEMPO-oxidized softwood and hardwood celluloses.

	Density (g/cm^3)	Moisture content (%)	Tensile strength (MPa)	Elastic modulus (GPa)	Elongation at break (%)
Softwood TOCN-film	1.46	13	233 ± 44	6.9 ± 1.4	7.6 ± 0.2
Hardwood TOCN-film	1.45	15	222 ± 11	6.2 ± 1.6	7.0 ± 2.4

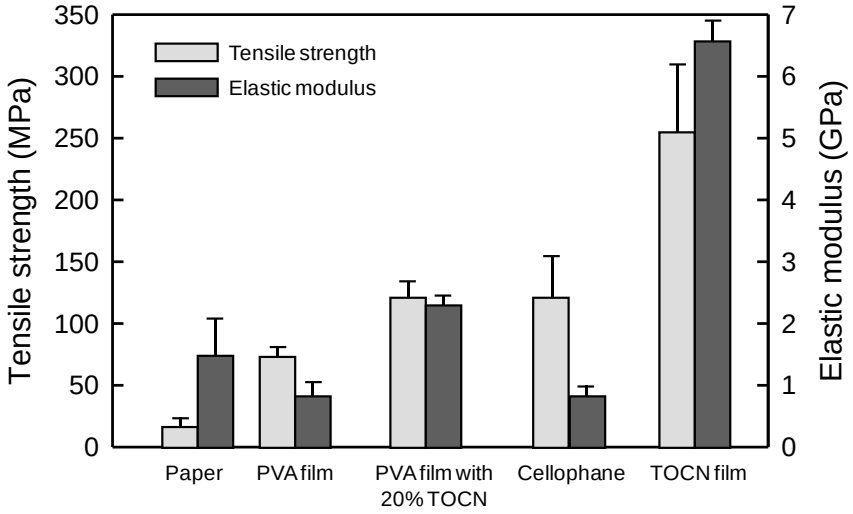

Figure 2.5. Tensile strengths and elastic modulus of TOCN films, 20% TOCN/PVA composite films and other references.

2.3.5 Oxygen-barrier properties

A polylactic acid (PLA) film surface-coated with TOCN was subjected to oxygen permeability determination at 0% R.H. The unmodified PLA film had an oxygen transmission rate of about 7.4 mL m^{-2} day^{-1} kPa^{-1}. Surprisingly, the oxygen transmission rate was decreased to 9.9×10^{-4} mL m^{-2} day^{-1} kPa^{-1} (Figure 2.6) by the thin TOCN layer. The recommended oxygen transmission rate for modified atmosphere packaging for foods or medicines is below 0.1–0.2 mL m^{-2} day^{-1} kPa^{-1}.[11] The oxygen permeability of the TOCN-coated PLA film was close to the value for typical synthetic polymer films such as poly(vinylidene chloride) and polyethylene-poly(vinyl alcohol) copolymers that have high oxygen barrier functionality.[12] The high oxygen-barrier property of TOCN is probably caused by the dense structure of crystalline nanofibrils as observed in SEM image (Figure 2.1).

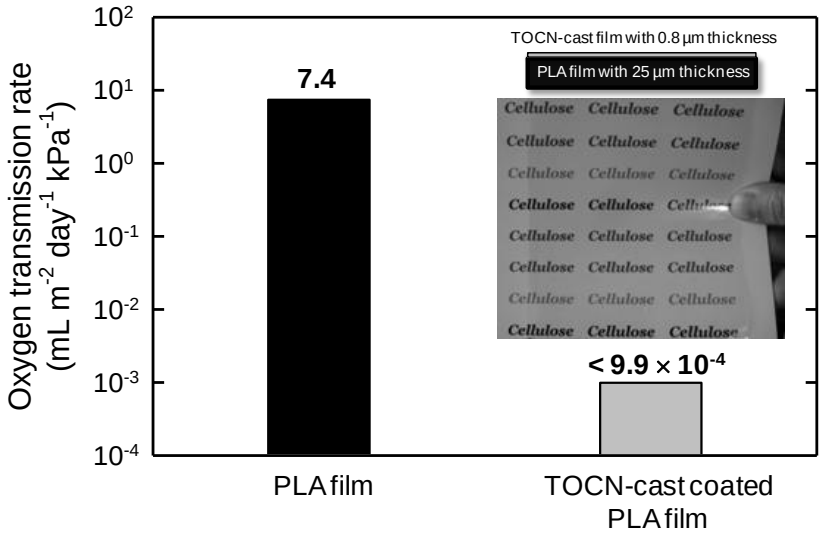

Figure 2.6. Transparency and flexibility of poly(lactic acid) (PLA) film coated with softwood TOCN film, and oxygen permeability values of the base PLA and TOCN/PLA films. The original PLA film was 25 µm in thick and the coated TOCN layer was 0.8 µm in thick.

The refractive index of PLA (1.48–1.50)[13] was close to that of TOCN (1.55). Therefore, transparent and highly oxygen-impermeable films can be obtained by coating

of TOCN dispersion on PLA films, which would make wholly biomass-sourced film packaging available for foods and medicines. The interaction or adhesion strength between PLA and TOCN layers at the interfaces in the TOCN-coated PLA films were improved by hydrophilic modification of the PLA surfaces by graft-polymerization treatment.[14]

2.3.6 Water-vapor permeability

As shown in Figure 2.7, water-vapor permeability (for 1 μm film thickness) of TOCN-cast films is quite high, in comparison with commercial films. The water-vapor permeability of commercial films were in good agreement with reported values.[15] Hydrophobic films such as PET, LDPE, and OPP had gentle slopes with increasing R.H., indicating that water molecule has no interaction during transfer though the polymers.[16] PLA displayed relatively high water-vapor permeability than for other hydrophobic films, but the water permeation in PLA is not yet completely understood yet.[12]

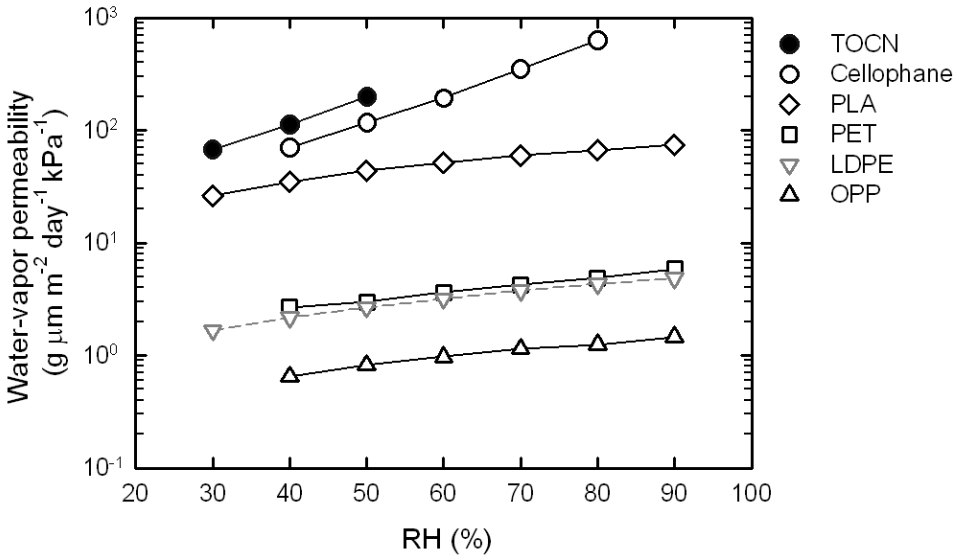

Figure 2.7. Water-vapor permeability of softwood TOCN, commercial cellophane, poly(ethylene terephthalate) (PET), low density poly(ethylene) (LDPE), and oriented poly(propylene) (OPP) films in various relative humidities.

On the other hand, hydrophilic cellophane and TOCN film draw exponential increase in water-vapor permeability with increasing R.H. Furthermore, the WVTRs at high R.H.

were too high to be measured because the transmission rates were over the upper limit for the measurement apparatus. The interaction sites of water molecules in cellulose must be hydroxyl groups, disordered regions, inner surfaces of voids and crystallites.[17] For the TOCN film, not only hydrophilic nature of cellulose, but also sodium carboxylate groups in the nanofibril surfaces cause the high water-vapor permeability, because the TOCN film with sodium carboxylate groups (TOCN-COONa) can adsorb much water than for the TOCN film with free carboxyl groups (TOCN-COOH).[10] For application in electronic or packaging fields, water sensitivity of TOCN is a drawback that needs to be improved.

2.3.7 Hydrophobization of TOCN film surface

The high carboxylate contents of TEMPO-oxidized wood celluloses (1.3–1.6 mmol g^{-1}), are necessary to convert wood cellulose fibers to TOCN films having the aforementioned characteristics, as well as to make water dispersions of completely separated nanofibrils.[1,2] However, the highly hydrophilic nature of the TOCN films may lead in turn to low resistance to water. The change in the contact angle with time of a water droplet placed on TOCN film was measured (Figure 2.8). Predictably, the original TOCN film was hydrophilic, and the initial water-contact angle was as low as 47°. The contact angle decreased with time as a result of partial penetration of water into the film or expanse of wetting. For comparison, the initial contact angles of cellophane and a glass plate were 33 and 48°, respectively, when measured under the same conditions.

Alkylketene dimer (AKD) is a typical hydrophobizing chemical used for paper. When an AKD dispersion is added to pulp fiber slurries, cationic AKD particles are efficiently adsorbed through electrostatic interactions on anionic sites or dissociated carboxyl groups originally present in wood cellulose fibers whose contents are 0.02–0.08 mmol g^{-1}.[18,19] TOCN film treated with a 0.05% AKD dispersion had water-contact angle of 94° and this value was maintained for at least 10 s. Transparency was maintained for the AKD-treated films. Thus, the hydrophilic TOCN films can be made hydrophobic using a simple soaking method with the cationic AKD dispersion.

The abundant carboxylate groups in TOCN film are likely to behave as adsorption sites for the cationic AKD dispersed particles. Consequently, the presence of significant amounts of carboxylate groups in the TOCN films is advantageous for efficient modification of the original properties of the films. It is noteworthy that surface hydrophobization of TOCN films was also observed by addition of small amount of AKD (0.05–1% for cellulose content) into 0.1% w/v TOCN/water dispersions. Cast and dried TOCN film containing 0.5% AKD exhibited a water-contact angle of about 100°.

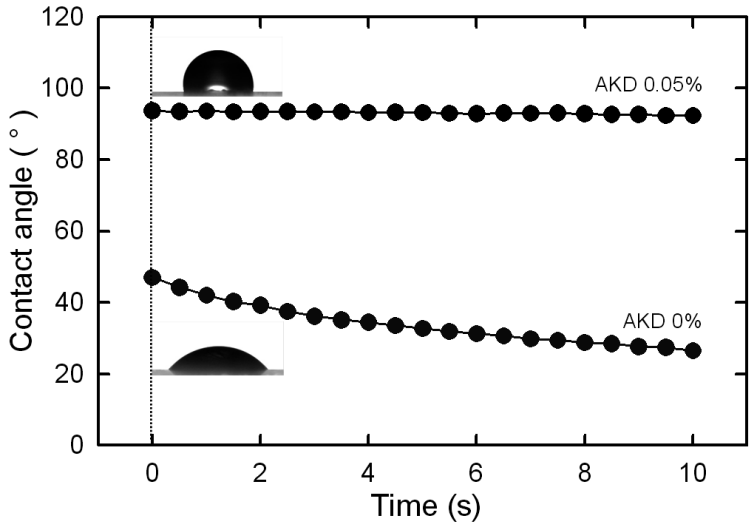

Figure 2.8. Change in the contact angle with time of a water droplet on nanofibril films prepared from TEMPO-oxidized softwood cellulose before and after treatment with a 0.05% alkyl ketene dimer dispersion.

2.4 Conclusion

TEMPO-oxidized cellulose nanofibril (TOCN) films prepared from softwood cellulose are transparent and flexible and have high tensile strength, substantially high oxygen barrier properties, and extremely low coefficient of thermal expansion caused by high crystallinity of native cellulose. The thermal degradation point of cellulose, however, decreased from 300 to 200 °C by the introduction of carboxylate groups through the TEMPO-mediated oxidation. Reinforcing effect was observed by addition

of 20% TOCN to poly(vinyl alcohol). Although the original TOCN films are hydrophilic and shows high water-vapor permeability, surface hydrophobization is achieved by a simple soaking treatment in the AKD dispersion. These unique characteristics of the TOCN films are promising for potential applications for flexible display panels, various electronic devices, and biomass-sourced packaging with high oxygen-barrier properties.

References

1. Saito, T.; Nishiyama, Y.; Putaux, J.-L.; Vignon, M.; Isogai, A. *Biomacromolecules*, **2006**, 7, 1687.
2. Saito, T.; Kimura, S.; Nishymama, Y.; Isogai, A. *Biomacromolecules*, **2007**, 8, 2485.
3. Saito, T.; Isogai, A. *Biomacromolecules*, **2004**, 5, 1983.
4. Saito, T.; Isogai, A. *Colloids Surf., A*, **2006**, 289, 219.
5. Iwamoto, S.; Isogai, A.; Iwata, T. *Biomacromolecules*, **2011**, 12, 831–836
6. Saito, T.; Uematsu, T.; Kimura, S.; Enomae, T.; Isogai, A. *Soft Matter*, **2011**, 7, 8804−8809.
7. Syverud, K.; Chinga-Carrasco, G.; Toledo, J.; Toledo, P. G. *Carbohydr. Polym.*, **2011**, 84, 1033–1038.
8. Nogi, M.; Yano, H. *Appl. Phys. Lett.*, **2009**, 94, 233117.
9. Paul, D. R.; Robeson, L. M. *Polymer*, **2008**, 49, 3187–3204.
10. Fujisawa, S.; Okita, Y.; Fukuzumi, H.; Saito, T.; Isogai, A. *Carbohydr. Polym.*, **2010**, 84, 579−583.
11. Syverud, K. ; Stenius, P. *Cellulose*, **2009**, 16, 75–85.
12. Lagaron, J. M.; Catalá, R.; Gavara, R. *Mater. Sci. Technol.*, **2004**, 20, 1−7.
13. Auras, R.; Harte, B.; Selke, S. *Macromol. Biosci.*, **2004**, 4, 835–864.
14. Kai, W.; Iwamoto, S.; Akamatsu, K.; Nakao, S.; Isogai A.; Iwata, T. *Polym. Degrad. Stab.*, **2010**, 95, 1004–1010.
15. Tock, R. W. *Adv. Polym. Tech.*, **1983**, 3, 223–231.

16. Morillon, V.; Debeaufort, F.; Capelle, M.; Blond, G.; Voilley A. *J. Agric. Food Chem.*, **2000**, 48, 11−16.
17. Belbekhouche, S.; Bras, J.; Siqueira, G.; Chappey, C.; Lebrun, L.; Khelifi, B.; Marais, S.; Dufresne, A. *Carbohyd. Polym.*, **2011**, 83, 1740–1748
18. Isogai, A.; Kitaoka, C.; Onabe, F. *J. Pulp Paper Sci.*, **1997**, 23, J215–J219.
19. Parks, E. J.; Hebert, R. L. *Tappi J.*, **1972**, 55, 1510.

CHAPTER 3

Pore size determination of TEMPO-oxidized cellulose nanofibril films by positron annihilation lifetime spectroscopy

3.1 Introduction

High oxygen-barrier properties are important for packaging films for foods and medicines to increase their shelf lives and for electronic devices, flexible display panels, and back-sealing materials for solar power generation systems. Petroleum-based polymer films such as poly(vinyl alcohol), ethylene-vinyl alcohol copolymer and poly(vinylidene chloride) containing clay nanoparticles or sputtered with aluminum or silicate are generally used as high oxygen-barrier materials.[1–8] Bio-based, environmentally friendly packaging films have been attracting great interest because most packaging material is discarded as burnable waste or used as landfill after use. In particular, various nano-fibrillated celluloses[9–19] and hemicelluloses[20–25] have the potential to be used as biodegradable oxygen-barrier films.

TEMPO-oxidized cellulose nanofibril (TOCN) is a candidate for the biodegradable oxygen-barrier film, which has transparency and flexibility. The high oxygen-barrier property of the film implies that no connected pore exists in the cross section of the film. Pore analysis is needed to understand the reason of the high oxygen-barrier property of the TOCN film. In this study, oxygen permeability (P_{O2}) values of self-standing and coated films of wood and tunicate TOCN-COONa and other related materials were measured, and positron annihilation lifetime spectroscopy (PALS) was used to determine pore sizes from the film surface to inside of the TOCN-COONa films.

In PALS technique, a positron emitted from radioactive sources (^{22}Na) is injected into a sample and forms a spin parallel bound state with an electron, which is called ortho-positronium (*o*-Ps). The *o*-Ps annihilates with an antiparallel electron of the surrounding medium to form gamma rays. The detected gamma rays of *o*-Ps annihilations exhibit the longest-lived component in the lifetime spectrum. The lifetime

of an *o*-Ps depends on the electron density in its local environment, which is sensitive to the size of the free volume. The PALS techneque has been widely adopted for study of defects in crystalline solids since 1970s.[26] The procedure for obtaining the pore size from positron lifetime measurements is well established and has been successfully applied to quantify pore sizes in various polymers.[27–32]

3.2 Experimental section

3.2.1 Materials

TEMPO-oxidized cellulose was prepared from a never-dried softwood bleached kraft pulp according to the method written in Experimental section 2.2.2. The TEMPO-oxidized cellulose was reacted with sodium chlorite (10 mmol) in an acetate buffer at pH 4.5 and room temperature for 1 day to oxidize C6-aldehyde groups that are present in the TEMPO-oxidized cellulose to carboxylate groups.[33] The weight recovery ratio and carboxylate content of the TEMPO-oxidized cellulose obtained after several treatments were ~90% and 1.4 mmol g^{-1}, respectively. TEMPO-oxidized wood cellulose with free carboxyl groups was prepared from the TEMPO-oxidized cellulose with sodium carboxylate groups by a previously reported procedure under acidic conditions.[15] TEMPO-oxidized tunicate cellulose with a sodium carboxylate content of 0.6 mmol g^{-1} was prepared from the purified outer skin of *Halocynthia roretzi*.[34] Cellouronic acid [sodium (1,4)-β-D-polyglucuronate] with a weight-average degree of polymerization of 320 was prepared from a commercial regenerated cellulose (Bemliese®, Asahi Chemicals) by the TEMPO/NaClO/$NaClO_2$ system at pH 6.8 according to a reported method.[35] Commercial cellophane containing glycerol as a plasticizer (Rengo, Tokyo, Japan), poly(ethylene terephthalate) films (Tetron G2, Teijin), and microfibrillated wood cellulose (2% solid content; Celish, Daicel Chemicals)[36] were used as received.

3.2.2 Preparation of TOCN films

A 0.15 w/v % TEMPO-oxidized cellulose/water slurry at pH 8 (50 mL) was disintegrated using an ultrasonic homogenizer (probe tip diameter: 7 mm; US-300T, Nissei) at a frequency of 19.5 kHz and an output power of 300 W for 8 min to obtain a transparent TOCN/water dispersion. The TOCNs had width of 3–4 nm and average length of 600 nm according to TEM observations. Self-standing wood TOCN-COONa films that were 11.07 ± 0.80 μm thick were prepared by casting the dispersion onto a poly(styrene) Petri dish and drying at 40 °C for 1 day. Some of these TOCN-COONa films were subsequently heated at 150 °C for 0.5 h. The surface of one side of the commercial PET film (thickness: 50 μm; area 9×9 cm^2) was hydrophilized by irradiating it with a plasma at 5 mA for 5 min in vacuum using a soft-etching device (DSDE-AF, Meiwafosis). The 0.15 w/v % wood TOCN-COONa/water dispersion (3, 5, or 7 mL) was uniformly cast onto the hydrophilized surface of the PET film and allowed to dry at room temperature for 3 days. Tunicate TOCN-COONa, wood TOCN-COOH, cellouronic acid-COONa, and microfibrillated cellulose were also cast onto hydrophilized PET films in a similar manner as described above.

3.2.3 Positron annihilation lifetime spectroscopy (PALS)

An experimental setup based on a pulsed slow-positron beam with variable energy intensity at the National Institute of Advanced Industrial Science and Technology (Tsukuba, Japan) was used to obtain PALS spectra and lifetime–energy correlation data of TOCN-COONa self-standing films in vacuum. The mean implantation depth (Z_0) as a function of incident positron energy was calculated using the following equation,[26,37] which has been applied to polymer films.[38–40]

$$Z_0 = 40\frac{E^{1.6}}{\rho}$$

where Z_0 is expressed in nm, ρ is the film density in g cm^{-3}, and E is the incident positron energy in keV. In this study, the incident positron energy was varied between 1 and 15 keV, which correspond respectively to mean depths of 26.5 and 1996 nm from

the film surface (assuming that wood TOCN-COONa films have a density of 1.47 g cm^{-3}.[15] Details of PALS system have been reported elsewhere.[41–45] The relationship between the *o*-Ps lifetime and the effective pore radius ($r \leq 1$ nm) is given by the following equation, which is based on a semi-empirical spherical-cavity model.[46–49]

$$\tau_3 = 0.5\left[1 - \frac{r}{r+0.166} + \frac{1}{2\pi}\sin\left(\frac{2\pi r}{r+0.166}\right)\right]^{-1}$$

where τ_3 (ns) represents the annihilation lifetime of the longest-lived *o*-Ps component and 2*r* (nm) is the pore diameter.

3.2.4 General Analyses

Images of the TOCN film surfaces were acquired using an atomic force microscope (AFM) in tapping mode (SPI 3800N and SI-DF20 Si cantilever, Seiko Instruments). Oxygen permeability measurements of self-standing and coating films were performed by Mocon OX-TRAN (Modern Controls) at 23 °C and 0% and 50% R.H. according to the standard method (ASTM 3985).[10,15] The film was cut to a suitable size and the oxygen transmission rates (OTRs) were measured for areas of 5 or 50 cm^2 at atmospheric pressure. Each sample was conditioned in the chamber of an OTR system for 3 h and the OTR was measured over 1–3 days until it reached a stable value. The oxygen permeability (P_{O2}) was obtained by multiplying the OTR by the film thickness. The P_{O2} of the TOCN layer in the TOCN/PET film (*i.e.*, P_{O2}(TOCN)) was calculated using the following equation:

$$\frac{T(TOCN/PET)}{P_{O2}(TOCN/PET)} = \frac{T(TOCN)}{P_{O2}(TOCN)} + \frac{T(PET)}{P_{O2}(PET)}$$

where *T* is the thickness of the TOCN layer, PET film, or TOCN/PET film. Film thicknesses were determined by the interference fringe technique,[50,51] which was performed on reflectance spectra of the films recorded with an UV–vis spectrophotometer (Jasco, V-670).

3.3 Results and discussion

3.3.1 Oxygen transmission rates of TOCN-COONa films

Figure 3.1 shows the relationship between the wood TOCN-COONa film thickness and the OTR for three TOCN-COONa/PET films and one self-standing TOCN-COONa film at 0% R.H. The standard deviations of the thicknesses of TOCN-COONa layers coated on the PET film were within ± 1.4%, whereas that of the self-standing TOCN-COONa films was ± 7%. Thus, the TOCN-COONa/PET films had more uniform thicknesses. From the slope of the line in Figure 3.1, the normalized OTR of TOCN-COONa films with thickness of 1 μm was estimated to be ~0.0008 mL m^{-2} day^{-1} kPa^{-1} at 0% R.H. This P_{O2} value is much lower than those of ethylene vinyl alcohol copolymer (EVOH) films (0.01 to 0.1 mL μm m^{-2} day^{-1} kPa^{-1}) at 0% R.H.[52]

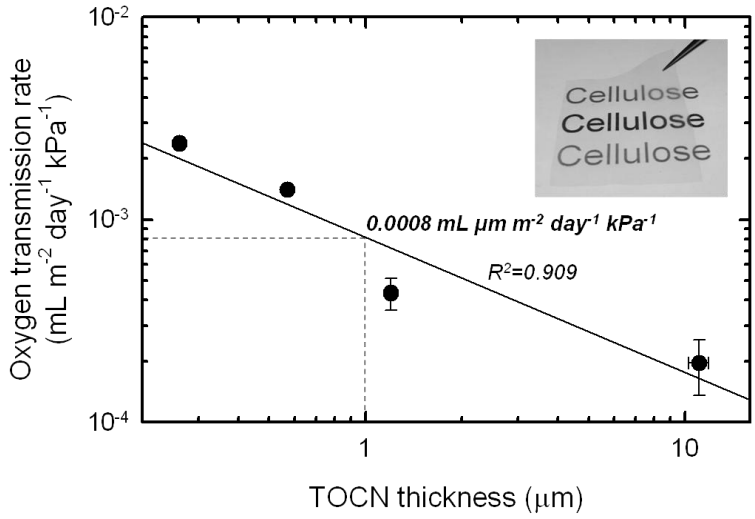

Figure 3.1. Oxygen transmission rates of wood TOCN-COONa films with various thicknesses. One self-standing film and three PET films coated with TOCN-COONa were measured at 0% R.H.

3.3.2 Oxygen permeabilities of various films

The P_{O2} values of various TOCN-related and reference films were measured at either 0% or 50% R.H. (Figure 3.2). The wood TOCN-COONa film heated at 150 °C for 0.5 h had a similar P_{O2} value to unheated films, indicating that the pore structure of the films

is largely unchanged by the heat treatment. The lower P_{O2} value of wood TOCN-COONa films relative to that of wood TOCN-COOH films has been reported in an earlier study.[15] The anionically charged wood TOCN-COONa elements dispersed in water probably results in close packing of the nanoelements during film formation by drying.[53] Because cellouronic acid-COONa films have much higher P_{O2} values than the wood TOCN-COONa films, crystalline TOCN-COONa elements may contribute significantly to the oxygen-barrier properties of the films.

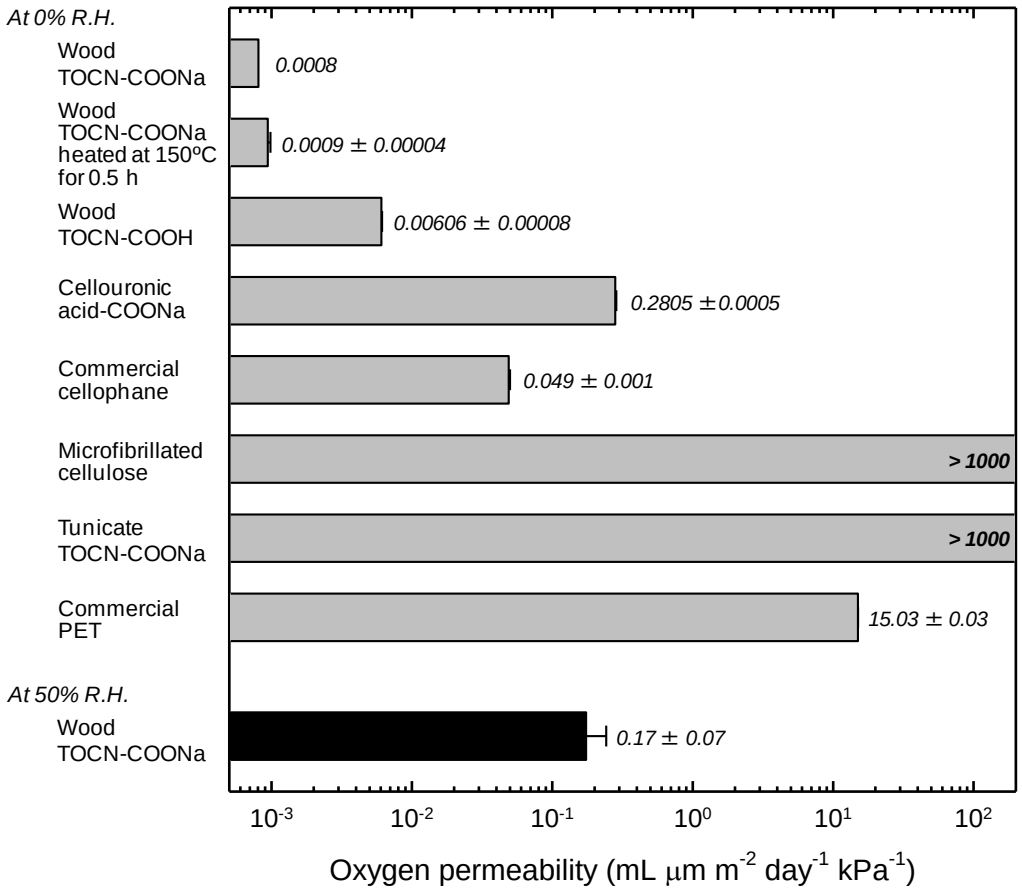

Figure 3.2. Oxygen permeabilities determined at 0% and 50% R.H. of wood TOCN-COONa film dried at 40 °C, a wood TOCN-COONa film heated at 150 °C for 0.5 h, a wood TOCN-COOH film,[15] a cellouronic acid-COONa film, a commercial cellophane,[19] a microfibrillated cellulose film, a tunicate TOCN-COONa, and a PET film.

Cellophane has a low crystallinity of cellulose II different from highly crystalline cellulose I structures of the TOCN films. Commercial cellophane containing glycerol as a plasticizer had a P_{O2} value of ~0.049 mL μm m^{-2} day^{-1} kPa^{-1}; the P_{O2} value decreased to ~0.010 mL μm m^{-2} day^{-1} kPa^{-1} after glycerol had been removed. Thus, the glycerol in cellophane increases the P_{O2} value at 0% R.H. The increase in oxygen permeability with the addition of glycerol was already observed for cellulosic films, and considered that it was attributed to enhanced oxygen solubility by plasticization. [13]

Microfibrillated cellulose (MFC) and tunicate TOCN-COONa self-standing and coated films exhibited almost no oxygen-barrier property. The MFC consists of not only cellulose nanofibrils but also fibril bundles and unfibrillated fibers with widths of 10–100 nm. Many researchers have reported P_{O2} values of MFCs. Rodionova et al. and Syverud et al. reported that the P_{O2} values were 1.74 and 3.52–5.03 mL μm m^{-2} day^{-1} kPa^{-1} at 0% and 50% R.H., respectively.[11,17] Belbekhouche et al. reported the greater values of 58.3 mL μm m^{-2} day^{-1} kPa^{-1} for MFC films.[16] The MFC film used in this study may have lower dense structure than TOCN film and contain many pores between MFC fibrils.

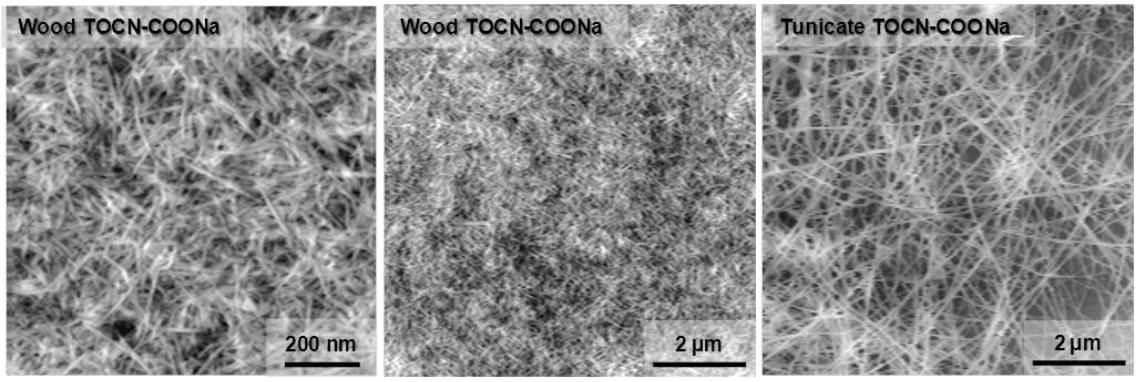

Figure 3.3. AFM images of surfaces of TOCN-COONa films prepared from wood and tunicate celluloses (observed in vacuum).

Figure 3.3 shows AFM images of wood and tunicate TOCN-COONa film surfaces at 0% R.H. Because the tunicate TOCN-COONa film consists of stiff cellulose nanofibrils with high aspect ratios,[54] there may be though holes from the top to bottom of the films,

resulting in almost no oxygen-barrier properties. Instead, the wood TOCN-COONa film surfaces had denser structures consisting of nanofibril elements with smaller widths and smaller aspect ratios. A previous study found that the cross sections of the wood TOCN-COONa films consisted of domains of uniaxially aligned TOCN-COONa elements with different orientation angles, which formed layers nearly parallel to the TOCN-COONa film surface.[55] Thus, the films have a plywood-like structure, which probably causes exceptionally high oxygen-barrier properties. Self-aligned structures of wood TOCN-COONa elements were not observed on the film surface (Figure 3.3), although a similar random fibril orientation to that in self-assembled cellulose microfibrils in plant cell walls was observed.[56]

The extremely low P_{O2} values of wood TOCN-COONa films at 0% R.H. increased to ~0.17 mL μm m^{-2} day^{-1} kPa^{-1} at 50% R.H., demonstrating that the hydrophilic nature of TOCN-COONa reduces the oxygen-barrier properties of the films. The wood TOCN-COONa films at 50% R.H. have comparable or higher P_{O2} values to those of ethylene vinyl alcohol copolymer and poly(vinylidene chloride) films at 50% R.H.[5,52] Moreover, almost no water-vapor barrier property was observed for the TOCN-COONa films at 90% R.H. It is thus essential to significantly improve both the oxygen and water-vapor barrier properties of TOCN-COONa films at high R.H. before wood TOCN-COONa films can be used as high gas-barrier packaging films. AFM images of wood TOCN-COONa film surfaces obtained at 0% and 50% R.H. were almost the same, indicating that there is no significant difference in the TOCN widths of the films at these two R.H. values.

3.3.3 PALS analysis of TOCN-COONa films

PALS analysis was applied to wood and tunicate TOCN-COONa self-standing films in vacuum at 0% R.H. Reliable data could not be obtained for the films at 50% R.H. All the lifetime spectra obtained in vacuum were best resolved into three components after subtracting the background and correcting for the positron source. The longest-lived component (τ_3) is due to the pick-off annihilation of *o*-Ps in the free volume sites. The

o-Ps lifetime (τ_3) is a measure of the pore size in polymers (a larger τ_3 indicates larger pores). The corresponding intensity (I_3) is indicative of the pore density in polymer (a higher I_3 indicates a higher pore density),[57,58] although this is not straightforward since complicated Ps formation processes determine the *o*-Ps intensity.

Figure 3.4 shows the dependence of the average pore size and corresponding o-Ps lifetime (τ_3) on the mean depth from top or bottom surface of the self-standing wood TOCN-COONa film determined by PALS in vacuum. The average pore size was approximately 0.47 nm and the pore size was almost constant from the film surface to depths up to ~2 μm from the film surface. This mean pore size is almost the same as those of EVOH films at 0% R.H.,[52,59] and slightly larger than kinetic diameter of O_2 molecules (0.346 nm). In addition, the PALS analysis revealed that no connected pore existed in the cross section of the film. Hence, the high oxygen-barrier property of the wood TOCN-COONa films is due to the crystalline structure of TOCNs and the small pore sizes in the films which are probably result of close packing of TOCNs.

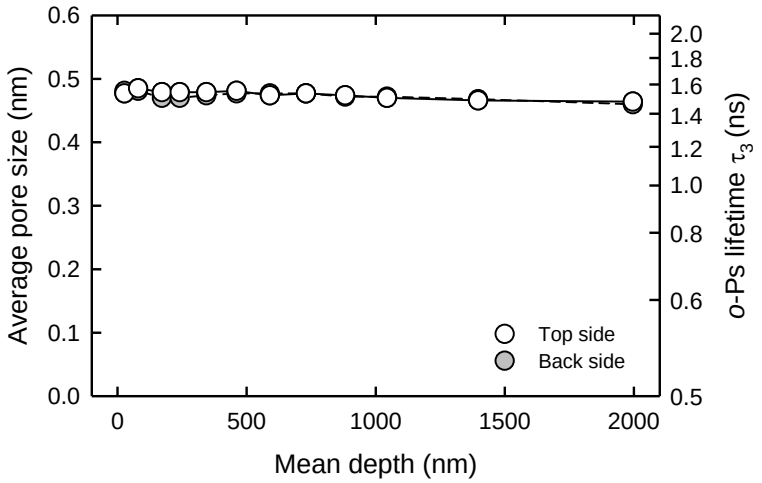

Figure 3.4. Dependence of pore size or *o*-Ps lifetime τ_3 on the mean depth from the top or bottom surface of a self-standing wood TOCN-COONa film determined by PALS in vacuum.

PALS analysis revealed that the mean pore size and its dependence on the mean depth from the film surface did not change when the film was heated to 150 °C for 0.5 h. This is consistent with the similar P_{O2} values for the heated and unheated films shown in

Figure 3.2. The pore sizes and structures formed in the wood TOCN-COONa films by drying at 40 °C probably do not change greatly on heating to 150 °C under dry conditions. On the other hand, heating or thermal drying wet TOCN-COONa films or gels at high temperatures may alter the pore size and structure. PALS analysis of the tunicate TOCN-COONa film gave average long-lived components (τ_3) long as 22–23 ns from the film surface to its interior, whereas that for the wood TOCN-COONa film was approximately 1.5 ns (Figure 3.4). The PALS data indicates the presence of through holes in the tunicate TOCN-COONa film so that the pore size calculation is inadequate in this case; shielding or capping of the surface with, for example, a SiO_2 or aluminum layer, is required to obtain accurate pore sizes for a closed-pore sample.[60,61] Regardless, the relatively high P_{O2} value of the tunicate TOCN-COONa film in Figure 3.2 is caused by the presence of through holes and large pores.

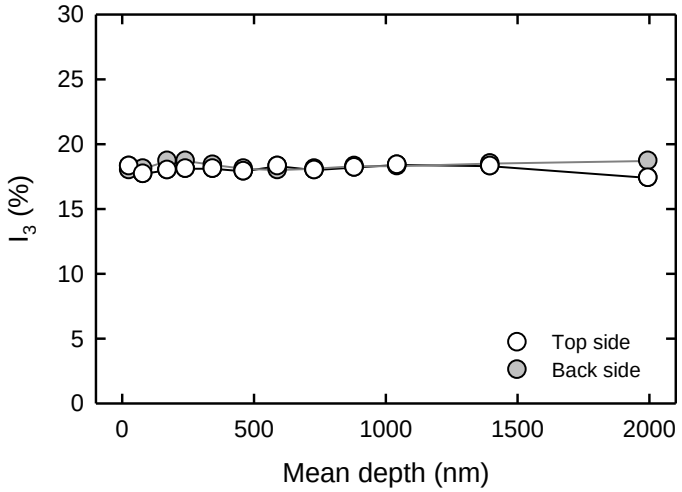

Figure 3.5. Dependence of intensity of the positron state 3 (I_3) on the mean depth from top or bottom surface of a self-standing wood TOCN-COONa film determined by PALS in vacuum.

Figure 3.5 shows the dependence of the intensity of the longest-lived component (I_3) on the mean depth of the self-standing wood TOCN-COONa film determined by PALS in vacuum. The *o*-Ps intensity varied slightly between 17 and 19% with the mean depth from the film surface, which indicates that the pores have an almost uniform distribution with depth. The wood TOCN-COONa film heated at 150 °C for 0.5 h also

had I_3–mean depth profiles that were almost identical to those of the unheated film shown in Figure 3.5. Therefore, the key factors responsible for the extremely high oxygen-barrier properties of the wood TOCN-COONa films at 0% R.H. are the crystalline structure of TOCNs, relatively small and uniform pore sizes of ~0.47 nm from the film surface to the interior, and probably the homogeneous pore distribution in the film.

3.3.4 Oxygen-barrier property of wood TOCN-COONa films

Table 3.1 shows P_{O2} values of wood TOCN-COONa compared with literature values for nano-sized celluloses prepared from wood. Interestingly, P_{O2} of MFCs is strongly influenced by surface pretreatment. The carboxymethylated MFC has comparable gas-barrier property to TOCN. The lower P_{O2} values of surface charged MFCs are often explained by the smaller fibril width, which may cause more packing structure in films, than untreated MFCs.[12,13]

Table 3.1. Oxygen permeability values of cellulose nanofibril and nanowhisker films. Oxygen permeability values in units of mL μm m^{-2} day^{-1} kPa^{-1} were calculated based on data in the cited references.

Materials	Fibril width	Fibril length	Test condition	Oxygen permeability (mL μm m^{-2} day^{-1} kPa^{-1})	Reference
TEMPO-oxidized cellulose nanofibrils (Wood TOCN-COONa)	3−4 nm	ca. 600 nm	23 °C, 0%RH	0.0008	This study
			23 °C, 50%RH	0.17	This study
Microfibrillated cellulose (untreated)	> 10 nm	–	23 °C, 50%RH	3.52–5.03	[11] Syverud et al. 2009
	–	–	0%RH	1.74	[16] Rodionova et al. 2011
	37–67 nm	–	25 °C	58.3	[15] Belbekhouche et al. 2011
Microfibrillated cellulose (enzymatic pretreated)	17–30 nm	Range of μm	35 °C, 0%RH	0.0051	[13] Minelli et al. 2010
Microfibrillated cellulose (carboxymethylated)	5–15 nm	Range of μm	35 °C, 0%RH	0.012	[13] Minelli et al. 2010
	5–10 nm	Several μm	23 °C, 0%RH	0.0006	[12] Aulin et al. 2010
			23 °C, 50%RH	0.85	[12] Aulin et al. 2010
	min 3–5 nm, max 25–30 μm	Several μm	23 °C, 50%RH	0.365–0.493	[17] Siro' et al. 2011
Microfibrillated cellulose (acetylated)	–	–	0%RH	2.66–4.60	[16] Rodionova et al. 2011
Cellulose nanowhisker	3.5–6.5 nm	148–282 nm	25 °C	90700	[15] Belbekhouche et al. 2011

The surface of cellulose nanowhisker (CNW) is slightly charged as presence of $-OSO_3$ groups.[62] The fibril width of CNW is almost the same as TOCN and carboxymethylated MFC. However, CNW film has almost no oxygen-barrier property. Belbekhouche et al. speculated that the lower aspect ratio and the lower packing of the CNW increased porosity in films than MFC which is composed of entangled fibrils with high aspect ratio.[15] In order to consider the oxygen-barrier of self-assembled nano-sized celluloses, size and surface chemistry of nano-sized celluloses are important factors.

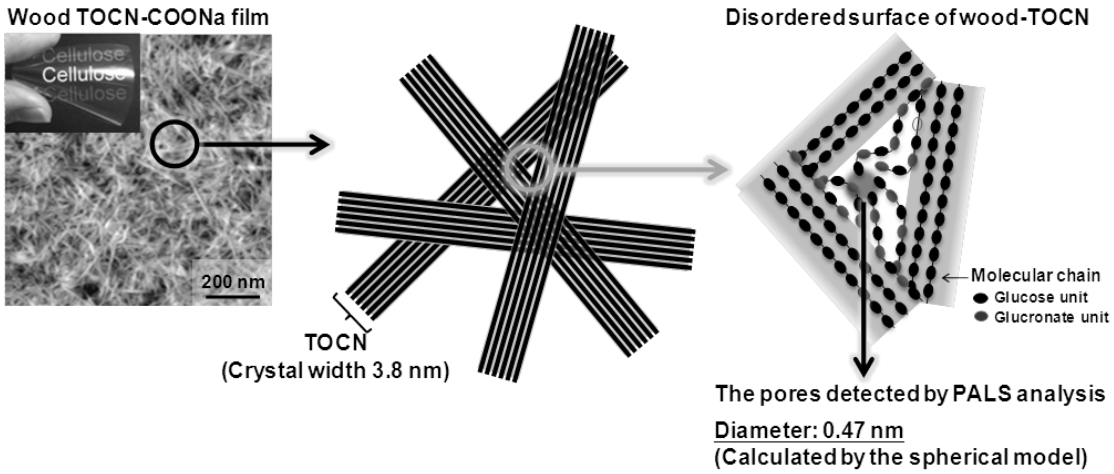

Figure 3.6. Schematic model of pores between wood-TOCN nanofibrils. The crystal width of wood-TOCN was cited from the reference.[34]

It is well known that the crystalline regions of a polymer film are impermeable. As for TOCN film, diffusion path of oxygen molecules is pores between nanofibrils. Okita et al. suggested that for higher plant celluloses; not only cellulose crystal surfaces but also amorphous or disordered regions were oxidized by TEMPO oxidation, and some of such oxidized parts may be retained in the solid celluloses without dissolving out in water.[34] Thus, the wood TOCNs may have some disordered structure on the nanofibril surface, as observed in crystal surface of plant cellulose.[63] Based on these previous findings, a speculative model of pore structure of the TOCN film was illustrated in Figure 3.6. The mobility of molecular chains in the disordered regions is restricted by surrounding crystal parts of the nanofibrils. In addition, the molecular chains in the

disordered regions may interconnect each other by hydrogen bonding at dry condition, and thus, the pore size detected by PALS analysis resulted in as small as that for EVOH film. At 50% R.H., however, the mobility may increase by moisture. Muramatsu et al. confirmed good correlations between P_{O2} and free volume hole size of EVOH at different temperatures and humidities.[52] Although the surface structure of the TOCN film observed by AFM were unchanged between 0% and 50% R.H, the pore sizes of the TOCN film might be increased with increasing R.H. because P_{O2} values were increased.

3.4 Conclusion

Coated and self-standing wood TOCN-COONa films have extremely low P_{O2} values of 0.0008 mL μm m^{-2} day^{-1} kPa^{-1} at 0% R.H. over a wide range of thickness. This was the lowest P_{O2} value obtained for wood TOCN-COOH, tunicate TOCN-COONa, and other tested films. However, the P_{O2} value of the wood TOCN-COONa film increased to 0.17 mL μm m^{-2} day^{-1} kPa^{-1} at 50% R.H. due to the hydrophilic nature of TOCN-COONa. PALS analysis revealed that the wood TOCN-COONa film had a constant pore size of ~0.47 nm from the film surface to the interior and that the pore distribution was probably homogeneous in the film at 0% R.H. The small pore size of the film and the crystalline structures of TOCN are probably responsible for the high oxygen-barrier properties of wood TOCN-COONa films at 0% R.H.

References

1. Miller, K. S.; Krochta, J. M. *Trends Food Sci. Technol.*, **1997**, 8, 228–237.
2. Cussler, E. L.; Hughes, S. E.; Ward III, W. J.; Aris, R. *J. Membr. Sci.*, **1988**, 38, 161–174.
3. Alexandre M.; Dubois, P. *Mat. Sci Eng. R*, **2000**, 28, 1–63.
4. Ray, S. S.; Okamoto, M. *Prog. Polym. Sci.*, **2003**, 28, 1539–1641.
5. Lange, J.; Wyser, Y. *Packag. Tehcnol. Sci.*, **2003**, 16, 149–158.

6. Usuki, A.; Hasegawa, N.; Kato, M.; Kobayashi, S. *Inorg. Polym. Nanocomp. Membr.*, **2005**, 179, 1–24.
7. Jørgensen, M.; Norrman, K.; Krebs F. C. *Sol. Energ. Mat. Sol. C.*, **2008**, 92, 686–714.
8. Choudalakis, G.; Gotsis, A. D. *Eur. Polym. J.*, **2009**, 45, 967–984.
9. Henriksson, M.; Henriksson, G.; Berglund, L. A.; Lindström, T. *Eur. Polym. J.*, **2007**, 43, 3434–3441.
10. Fukuzumi, H.; Saito, T.; Iwata, T.; Kumamoto, Y.; Isogai, A. *Biomacromolecules*, **2009**, 10, 162–165.
11. Syverud, K.; Stenius, P. *Cellulose*, **2009**, 16, 75–85.
12. Aulin, C.; Gallstedt, M.; Lindström, T. *Cellulose*, **2010**, 17, 559–574.
13. Minelli, M.; Baschetti, M. G.; Doghieri, F.; Ankerfors, M.; Lindström, T.; Siró, I.; Plackett, D. *J. Membr. Sci.*, **2010**, 358, 67–75.
14. Hult, E. L.; Lotti, M.; Lenes, M. *Cellulose*, **2010**, 17, 575–586.
15. Fujisawa, S.; Okita, Y.; Fukuzumi, H.; Saito, T.; Isogai, A. *Carbohydr. Polym.*, **2010**, 84, 579–583.
16. Belbekhouche, S.; Bras, J.; Siqueira, G.; Chappey, C.; Lebrun L.; Khelifi, B.; Marais, S.; Dufresne, A. *Carbohydr. Polym.*, **2011**, 83, 1740–1748.
17. Rodionova, G.; Lenes, M.; Eriksen, O.; Gregersen, O. *Cellulose*, **2011**, 18, 127–134.
18. Siró, I.; Plackett, D.; Hedenqvist, M.; Ankerfors, M.; Lindström, T. *J. Appl. Polym. Sci.*, **2011**, 119, 2652–2660.
19. Yang, Q.; Fukuzumi, H.; Saito, T.; Isogai, A.; Zhang, L. *Biomacromolecules*, **2011**, 12, 2766–2771.
20. Smart, C.; Whistler, R. L. *Science*, **1949**, 110, 713–714.
21. Hartman, J.; Albertsson, A.-C.; Sjöberg, J. *Biomacromolecules*, **2006**, 7, 1983–1989.
22. Hartman, J.; Albertsson, A.-C.; Lindblad, M. S.; Sjöberg, J. *J. Appl. Polym. Sci.*, **2006**, 100, 2985–2991.

23. Hansen, N. M. L.; Plackett, D. *Biomacromolecules*, **2008**, *9*, 1494–1505.
24. Edlund, U.; Ryberg, Y. Z.; Albertsson, A.-C. *Biomacromolecules*, **2010**, 11, 2532–2538.
25. Ryberg, Y. Z.; Edlund, U.; Albertsson, A.-C. *Biomacromolecules*, **2011**, 12, 1355–1362.
26. Schultz, P. J.; Lyn, K. G. *Rev. Mod. Phys.*, **1989**, 60, 701–779.
27. Kobayashi, Y.; Zheng, W.; Meyer, E. F.; McGervery, J. D.; Jamieson, A. M.; Simha, R. *Macromolecules*, **1989**, 22, 2302–2306.
28. Kobayashi, Y.; Haraya, K.; Hattori, S.; Sasuga, T. *Polymer*, **1994**, 35, 925–928.
29. Schmidt, M.; Olsson, M.; Maurer, F. H. J. *J. Chem. Phys.*, **2000**, 112, 11095–11106.
30. Hagiwara, K.; Ougizawa, T.; Inoue, T.; Hirata, K.; Kobayashi, Y. *Radiat. Phys. Chem.*, **2000**, 58, 525–530.
31. Schmidt, M.; Mauer, F. H. J. *Polymer*, **2000**, 41, 8419–8424.
32. Nagel, C.; Günther-Schade, K.; Fritsch, D.; Strunskus, T.; Faupel, F. *Macromolecules*, **2002**, 35, 2071–2077.
33. Saito, T.; Isogai, A. *Biomacromolecules*, **2004**, 5, 1893–1989.
34. Okita, Y.; Saito, T.; Isogai, A. *Biomacromolecules*, **2010**, 11, 1696−1700.
35. Hirota, M.; Tamura, N.; Saito, T.; Isogai, A. *Carbohydr. Polym.*, **2009**, 78, 330–335.
36. Turbak, A. F.; Snyder, F. W.; K. Sandberg, K. R. *J. Appl. Polym. Sci., Appl. Polym. Symp.*, **1983**, 37, 815–827.
37. Kobayashi, Y.; Ito, K.; Oka, T.; He, C.; Mohamed, H. F. M., Suzuki, R.; Ohdaira, T. *Appl. Surface Sci.*, **2008**, 255, 174–178.
38. Algers, J.; Suzuki, R.; Ohdaira, T.; Maurer, F. H. J. *Polymer*, **2004**, 45, 4533–4539.
39. Chen, H.; Hung, W.-S.; Lo, C.-H.; Huang, S.-H.; Cheng, M.-L.; Liu, G.; Lee, K.-R.; Lai, J.-Y.; Sun, Y.-M.; Hu, C.-C.; Suzuki, R.; Ohdaira, T.; Oshima, N.; Jean, Y. C. *Macromolecules*, **2007**, 40, 7542–7557.
40. Tung, K.-L.; Jean Y. C.; Nanda, D.; Lee, K.-R.; Hung, W. S.; Lo, C.-H.; Lai, J.-Y. *J. Membr. Sci.*, **2009**, 343, 147–156.
41. Suzuki, R.; Ohdaira, T., Mikado, T.; Uedono, A.; Ohgaki, T.; Yamazaki, T.;

Tanigawa, S. *Mater. Sci. Forum*, **1997**, 114, 255–257.

42. Suzuki, R.; Ohdaira, T.; Mikado, T. *Radiat. Phys. Chem.*, **2000**, 58, 603–606.
43. Suzuki, R.; Ohdaira, T.; Kobayashi, Y.; Ito, K.; Shioya, Y.; Ishimaru, T. *Radiat. Phys. Chem.*, **2003**, 68, 339–343.
44. He, C.; Suzuki, R.; Ohdaira, T.; Oshma, N.; Kinomura, A.; Muramatsu, M.; Kobayashi, Y. *Chem. Phys.*, **2007**, 331, 213–218.
45. He, C.; Muramatsu, M.; Ohdaira, T.; Oshima, N.; Kinomura, A.; Suzuki, R.; Kobayashi, Y. *Radiat. Phys. Chem.*, **2007**, 76, 204–208.
46. Tao, S. J. *J. Chem. Phys.*, **1972**, 56, 5499–5510.
47. Eldrup, M.; Light body, D.; Sherwood, J. N. *Chem. Phys.*, **1981**, 63, 51–58.
48. Nakanishi, H.; Wang, S. J.; Jean, Y. C. *In* Positron Annihilation Studies of Fluids, Sharma, S. C., Ed., *World Scientific*: Singapore, 1988, p 292–298.
49. Positron and Positronium Chemistry, Jean, Y. C.; Schrader, D. M. Eds., *Elsevier*, Amsterdam, **1988**. [ISBN 0444430091, 9780444430090]
50. Mastromatteo, M.; Del Nobile, M. A. *J. Food Eng.*, **2011**, 102, 170–176.
51. Leterrier, Y. *Prog. Matter. Sci.*, **2003**, 48, 1–55.
52. Muramatsu, M.; Okura, M.; Kuboyama, K.; Ougizawa, T.; Yamamoto, T.; Nishihara, Y.; Saito, Y.; Ito, K.; Hirata, K.; Kobayashi, Y. *Radiat. Phys. Chem.*, **2003**, 68, 561–564.
53. Ohta, S.; Inasawa, S.; Koike, O.; Fujita, M.; Yamaguchi, Y. *Appl. Phys. Express*, **2009**, 2, 065002.
54. Iwamoto, S.; Kai, W.; Iwata, T.; Isogai, A. *Biomacromolecules*, **2009**, 10, 2571–2576.
55. Saito, T.; Uematsu, T.; Kimura, S.; Enomae, T.; Isogai, A. *Soft Matter*, **2011**, 7, 8804−8809.
56. Roland, J.-C., Reis, D.; Vian, B. *Tissue Cell*, **1992**, 24, 335–345.
57. Hsieh, T. T.; Tiu, C.; Simon, G. P. *Polymer*, **2000**, 41, 4737–4742.
58. Ammala, A.; Pas, S. J.; Lawrence, K. A.; Stark, R.; Webb, R. I., Hill, A. J. *J. Mater. Chem.*, **2008**, 18, 911–916.

59. Ito, K.; Saito, Y.; Yamamoto, T.; Ujihira, Y.; Nomura, K. *Macromolecules*, **2001**, 34, 6153–6155.
60. Kobayashi, Y.; Zheng, W.; Chang, T. B.; Hirata, K.; Suzuki, R.; Ohdaira, T.; Ito, T. *J. Appl. Phys.*, **2002**, 91, 1704–1706.
61. Maex, K.; Baklanov, M. R.; Shamiryan, D.; Iacopi, F.; Brongersma, S. H.; Yanovitskaya, Z. S. *J. Appl. Phys.*, **2003**, 93, 8793–8841.
62. Habibi, Y.; Lucia, L. A.; Rojas, O. J. *Chem. Rev.*, **2010**, 110, 3479–3500.
63. Larsson, P. T.; Hult, E.; Wickholm, K.; Pettersson, E.; Iversen, T. *Solid State Nucl. Magn. Reson.*, **1999**, 15, 31–40.

Chapter 3 Pore size determination of TEMPO-oxidized cellulose nanofibril films by positron annihilation lifetime spectroscopy

CHAPTER 4

Thermal stabilization of TEMPO-oxidized cellulose

4.1 Introduction

TEMPO-oxidized cellulose nanofibrils (TOCN) film had characteristic properties such as high transparency, high strength, low-thermal expansion and extremely low oxygen-permeability. Hence, TOCN have attracted attention as new bio-based nanofibers for highly functional packaging films, biodegradable composite materials, flat panel display films, etc. However, the presence of sodium carboxylate groups in TEMPO-oxidized cellulose nanofibrils (TOCN) decreased the thermal decomposition temperature (T_d) to 222 ºC from approximately 275 ºC for the original cellulose (See section 2.3.3). Improvement of thermal stability of TOCN is necessary for various applications, because most commercial films are produced as composites with other polymers, which are thermally plasticized in molding process. The objective of this chapter involves examinations of the impact of carboxylate groups present in TEMPO-oxidized cellulose (TOC) and TOC nanofibrils, methylation of carboxyl groups of TOC with trimethylsilyl diazomethane ($TMSCHN_2$),[1–5] and metal ion-exchange treatments[6] on thermal degradation behavior of TOC and its related materials.

Because T_d points of cellulose acetates have been reported to be in the range of 240–360 ºC depending on degrees of substitution,[7–9] esterification of carboxyl groups is expected to improve thermal stability of TOC. The effects of alkali, alkaline-earth and other metal salts mixed with cellulose and cellulose derivatives on their thermal degradation behavior have been investigated primarily for evaluation of thermal stability, improvement of flame retardancy and obtaining valuable low-molecular-weight compounds by catalytic thermal degradation.[10–16] The addition of alkali and alkaline-earth metal salts to cellulose decreased T_d points of cellulose,[16] and sodium and potassium ions rather than calcium ion enhanced catalytic thermal degradation of

cellulose.[11,14] When metal ions were introduced to wood pulps and cellulose derivatives as counter ions of carboxyl or phosphate groups by ion-exchange treatments, thermal degradation behavior was influenced, depending on the metal ions introduced.[17–23] T_d points of these anionic groups-containing celluloses with sodium ions increased by ion-exchange treatment with calcium ions,[22] and decreased by replacing them with aluminum or iron ions.[17,19] Thus, thermal stability of TOC is anticipated to be influenced by metal ions and their quantities introduced by the ion-exchange treatments.

4.2 Experimental section

4.2.1 Materials

2 M $TMSCHN_2$ in diethylether was a commercial product (Sigma-Aldrich, USA). TEMPO, sodium bromide, 13% sodium hypochlorite solution, sodium chlorite, cellulose triacetate and other chemicals were of laboratory grade (Wako Pure Chemicals, Co. Ltd, Japan), and used as received.

Never-dried softwood bleached kraft pulp with carboxyl content of 0.03 mmol g^{-1} was used as the cellulose sample. TEMPO-mediated oxidation was applied to the cellulose according to the method written in Experimental section 2.2.2. The TEMPO-oxidized cellulose thus obtained had sodium carboxylate and aldehyde contents of 1.53 and 0.15 mmol g^{-1}, respectively. To avoid unexpected reactions due to the aldehyde groups, the TEMPO-oxidized cellulose (1 g) was further subjected to oxidation with sodium chlorite (1.8 g) in 0.5 M acetate buffer (90 ml) at pH 4–5 and room temperature for 24 h. Carboxyl content of the TEMPO-oxidized cellulose increased to 1.68 mmol g^{-1} by this $NaClO_2$ oxidation. This fibrous TEMPO-oxidized cellulose (TOC) with no aldehyde groups was washed thoroughly with water by filtration, and stored in never dried state before further treatment. The TOC with free carboxyl groups (TOC-COOH) was prepared from TOC-COONa by soaking in 0.1 M HCl at room temperature for 2 h followed by filtration and washing thoroughly with water. A cast and dried film of the TOC nanofibrils with sodium carboxylate groups was

prepared from a TOC/water dispersion according to the Experimental section 2.2.3.

4.2.2 Alkali treatment of TEMPO-oxidized cellulose

Cellulose molecules containing anhydroglucuronate units in the TOC were tried to be removed as much as possible by repeated alkali treatments.[24] The fibrous TOC (1 g) was suspended in 1 M NaOH (100 ml), and the mixture was stirred at 100 ºC for 1.5 h followed by washing thoroughly with water using filtration. This alkali treatment was repeated four times. The alkali-treated TOC had carboxyl content of 0.23 mmol g^{-1}, and its sodium carboxylate groups were converted to free carboxyl groups by soaking in 0.1 M HCl at room temperature for 2 h followed by washing thoroughly with water using filtration. The weight recovery ratio of the alkali-treated TOC as a solid mass was approximately 60%.

4.2.3 Methylation of TEMPO-oxidized cellulose with $TMSCHN_2$

The never-dried TOC with free carboxyl groups (0.5 g) was successively subjected to solvent-exchange with ethanol and acetone, and then vacuum-dried to remove adsorbed water completely. The solvent-exchanged and then dried TOC with free carboxyl groups was stirred in a mixture of dehydrated dimethylsulfoxide (DMSO, 40 ml) and methanol (8 ml) in nitrogen flow. 2 M $TMSCHN_2$ (1.5 ml)[1–5] was added dropwise to the slurry, and the mixture was stirred at room temperature for 1 h. The methylation was stopped by adding 2 M acetic acid (1.5 ml) to the mixture. The fibrous fraction was washed successively with DMSO, ethanol and acetone by filtration. The methylated product thus obtained was dried in air, and then vacuum-dried.

4.2.4 Counter ion-exchange treatments

The TOC-COONa (0.3 g) was added to an aqueous solution (40 ml) containing 0.25 M metal salt, which corresponded to approximately 20 times as much as the mole of sodium carboxylate groups of the TOC in the slurry.[6] The pH values of the slurries were measured. After being stirred at room temperature for 2 h, the fibrous fraction of the

slurry was filtered and washed thoroughly with water. The TEMPO-oxidized celluloses having various metal carboxylate groups were then freeze-dried. The following metal salts were used for the ion-exchange treatments: potassium chloride, potassium iodide, magnesium chloride, calcium chloride, calcium acetate, calcium nitrate, calcium iodide, strontium chloride, strontium acetate, silver nitrate, nickel chloride, iron (III) chloride, aluminum chloride, and lanthanum chloride.

4.2.5 Analysis

Thermogravimetric (TG) analyses of the cellulosic samples were conducted by means of a Thermoplus TG8120 (Rigaku, Japan) with nitrogen flow and heating rates of 500 ml min^{-1} and 4 ºC min^{-1}, respectively. Approximately 1 mg of the sample was set in a platinum pan for the TG analysis. In this study, thermal decomposition (T_d) temperatures were defined as those at the 5% weight decrease in TG curves, and peak temperatures of derivative TG (DTG_{peak}) were obtained from the DTG curves by the conventional method.[25–27]

Carboxyl contents of cellulosic samples were calculated by conductivity titration according to the reported method.[28]

TEMPO-oxidized celluloses before and after methylation were converted into pellets by pressing at ~750 MPa for 1 min, and subjected to FT-IR analysis (FT/IR-6100, JASCO, Japan) by the ATR method and wide-angle X-ray diffraction measurement (RINT 2000, Rigaku, Japan) by the reflection method with a monochromator-treated CuK_{α} radiation at 40 kV and 40 mA. Crystallinity index and crystal size of the (2 0 0) plane of cellulose I were calculated from the X-ray diffraction patterns according to the reported method.[28,29]

TEMPO-oxidized celluloses having metal carboxylate groups were subjected to X-ray fluorescence analysis (MESA-500, HORIBA, Japan) for determination of metal-ion contents.[6]

4.3 Results and discussion

4.3.1 Thermal degradation behavior of TEMPO-oxidized cellulose

Figure 4.1 shows TG and the corresponding DTG curves of the original cellulose, TEMPO-oxidized cellulose (TOC) with sodium carboxylate groups, and TOC nanofibril film with sodium carboxylate groups. The data is shown from 100 ºC to neglect the loss of water. The original cellulose (softwood bleached kraft pulp) exhibited the two-stage process of degradation as observed for literatures.[25,30] The first step of mass loss is a fast degradation starts at 275 ºC, and the second one is a slow degradation from 322 ºC. About 75% weight decreases during the first step. Although cellulose pyrolysis is a complicated process and the kinetics and chemistry of cellulose pyrolysis are still debated, it is generally accepted that the first step in the cellulose pyrolysis is mainly due to the depolymerization of solid cellulose to form levoglucosan (1,6-anhydro-b-D-glucose).[25–27]

Thermal decomposition (T_d) point of the TOC with sodium carboxylate groups (TOC-COONa) of 1.68 mmol g^{-1} was approximately 222 ºC, which was clearly lower than that of the original cellulose (275 ºC). Moreover, the cast and dried film of TOC nanofibrils also had T_d of 211 ºC. Both TOC-COONa and TOC-COONa nanofibrils had much slower degradation in the first step of mass loss than for original cellulose, and approximately 50% weight decreased during the first step. The second step of mass loss starts at 305 ºC and 301 ºC for TOC-COONa and TOC-COONa nanofibrils, respectively. Generally, uronic acids such as glucuronic and galacturonic acid have lower thermal stability than non-uronide sugers.[31,32] Britto et al. reported that carboxymethyl celluloses degraded at lower temperatures than cellulose due to decarboxylation of the sodium carboxyl groups.[22] Jakab et al. reported that partially carboxymethylated cellulose promoted decomposition of the carbohydrate chains leading to levoglucosan evolution at lower temperature.[23] Perlin reported that decarboxylation of uronic acid was observed at around 255 ºC, and almost theoretical quantities of carbon dioxide was detected at the same temperature.[33] Similar decarboxylation mechanism is likely to be applied also to the T_d of the TOC fibers and TOC nanofibril films.

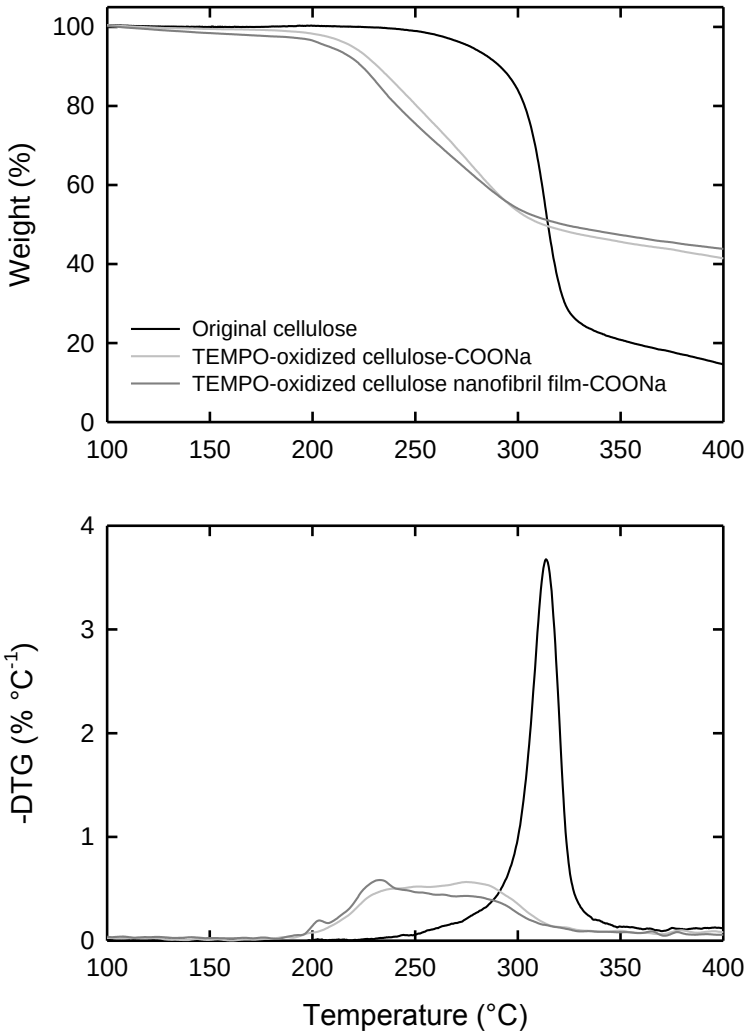

Figure 4.1. Thermogravimetric (upper) and the corresponding derivative thermogravimetric (DTG) (lower) curves of the original cellulose, TEMPO-oxidized cellulose (TOC) with sodium carboxylate groups and TOC nanofibril film with sodium carboxylate groups.

The DTG curves of the fibrous TOC-COONa and the TOC-COONa nanofibril film were broad, and seemed to consist of mainly two peaks around 233 ºC and 282 ºC. The former is probably due to the degradation of sodium anhydroglucuronate units, because cellouronic acid [sodium (1,4)-β-D-polyglucuronate] has DTG_{peak} at the same temperature (The data is not shown here). The latter DTG_{peak} is clearly lower than that of the original cellulose (313 ºC), indicating that cellulose chains in the crystal core

degrades around the DTG_{peak} points by the effect of thermally more unstable anhydroglucuronate units present in the crystal surface. In addition, the cast film of TOC-COONa nanofibrils start to degrade slightly earlier than TOC-COONa and have small DTG_{peak} around 205 ºC. It may be attributed to the efficient heat transfer of TOC-COONa nanofibrils, which have increased surface area by disintegration from fibrils to nanofibrils.

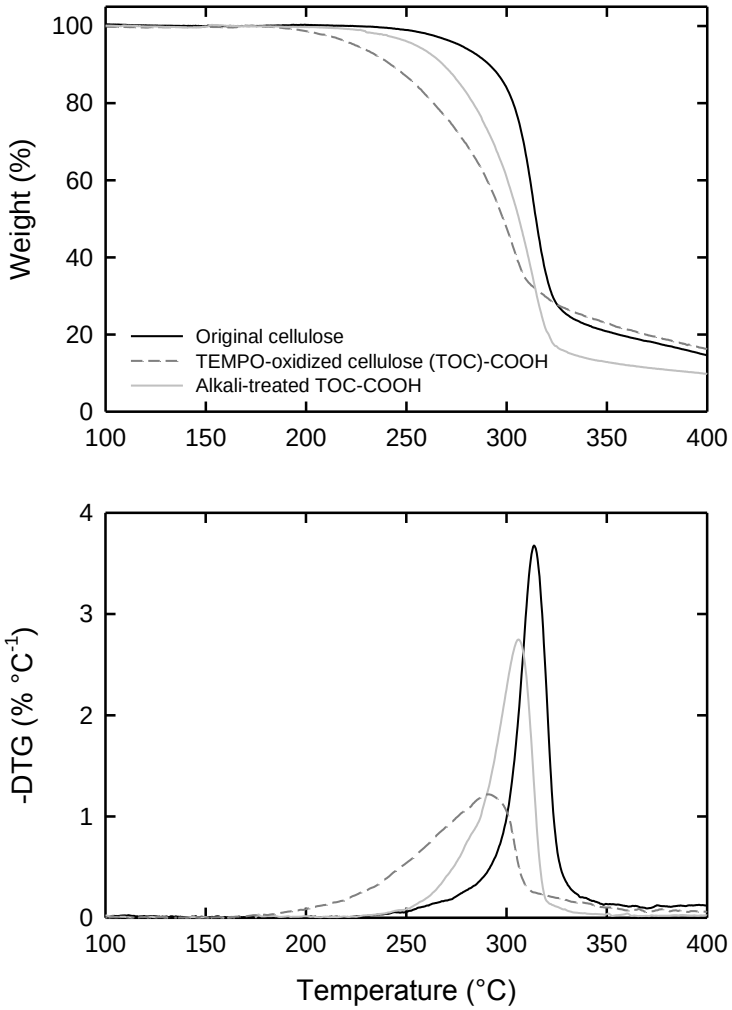

Figure 4.2. Thermogravimetric (upper) and the corresponding derivative thermogravimetric (DTG) (lower) curves of the original cellulose, TEMPO-oxidized cellulose (TOC) with free carboxyl groups of 1.68 mmol g^{-1} and alkali-treated TOC with free carboxyl groups of 0.23 mmol g^{-1}.

The influence of anhydroglucuronic acid units in the TOC on T_d values was further studied by the alkali treatment. The oxidized cellulose chains having the anhydroglucuronic acid units were tried to be removed from the fibrous TOC as much as possible by the repeated treatments of degradation and extraction with 1 M NaOH at 100 ºC for 1.5 h, whereas the crystalline cellulose regions present inside each TOC microfibril remained as solids.[24] As described in the Experimental section 4.2.2, carboxyl content was decreased from 1.68 mmol g^{-1} to 0.23 mmol g^{-1} by the alkali treatment; approximately 86% of the carboxyl groups were removed while maintaining the fibrous morphology. Crystal size of cellulose was decreased from 4.05 nm to 3.68 nm by the alkali treatment. In this section, T_d temperatures were determined for the samples with free carboxyl groups instead of sodium carboxylate groups. Figure 4.2 shows the TG and the corresponding DTG curves of TOC with free carboxyl groups (TOC-COOH), alkali-treated TOC-COOH, and together with those of the original cellulose. T_d point of TOC-COOH was 226 ºC, which was close to that of TOC-COONa (222 ºC, Figure 4.1). The structural difference between the sodium carboxylate and free carboxyl groups in the TOC had little influence on the T_d points. On the other hand, the DTG_{peak} of TOC-COOH was 292 ºC, which was slightly shifted to higher temperature compared with those of TOC-COONa. The DTG_{peak} at around 233 ºC observed in TOC-COONa (probably the degradation of the sodium anhydroglucuronate units) was ambiguous in the DTG curve of TOC-COOH. In addition, weight which decreased in the first step of weight loss were 65% and 50% for TOC-COOH and TOC-COONa, respectively. The difference in weight of remaining was due to the mass difference of hydrogen and sodium. The 86% removal of the carboxyl groups in the fibrous TOC by the alkali treatment followed by conversion of the residual sodium carboxylate groups to free carboxyl groups resulted in an increase in T_d point to 264 ºC. Alkali-treated TOC-COOH had DTG_{peak} at 312 ºC, which was higher than that of TOC-COOH. Therefore, the anhydroglucuronate and/or anhydroglucuronic acid units present in the crystal surface of TOC have strong influence on T_d even unoxidized cellulose chains present in the crystal core. The difference between the sodium carboxylate and free

carboxyl groups gives little influence on the initial T_d temperature. Because T_d behaviors of TOC and TOC nanofibril film were roughly the same (Figure 4.1), TOC was used as the original sample in the subsequent sections.

4.3.2 The effect of methylation

Methylation of carboxyl groups in the fibrous TOC with $TMSCHN_2$ was studied to improve thermal stability, because cellulose triacetates had T_d and DTG_{peak} of 292 ºC and 337 ºC, respectively, as described later, and were much higher than those of the fibrous TOC-COONa. Decarboxylation was, thus, expected to be retarded to some extent by converting the carboxyl groups to methyl ester groups. $TMSCHN_2$ is a stable methylation reagent substitute for diazomethane. Methylation of carboxyl groups by $TMSCHN_2$ can proceed at room temperature in high yields, which is suitable for use in gas-chromatographic analyses of carboxyl groups-containing compounds.[1–5] It is well known that methylation takes place not only carboxyl groups but also some hydroxyl groups of cellulose, when methylation is carried out with diazomethane in, for example, diethylether containing even a small amount of water.[3,5] Thus, in this study, the presence of water in the methylation media was avoided as much as possible using dry samples and dehydrated solvents. Tot et al. recently applied the $TMSCHN_2$ methylation to cellulosic pulps, and revealed that no depolymerization occurred during methylation.[5] Moreover, only carboxyl groups present as uronic acid moieties in hemicelluloses were selectively methylated in high ratios.[5] The weight recovery ratio after the methylation was 96% in this study, and no clear morphological changes of the fibrous TOC were observed before and after the methylation.

X-ray diffraction patterns of the original cellulose, the alkali-treated TOC with free carboxyl groups and the carboxyl groups-methylated TOC are depicted in Figure 4.3. In both the alkali and methylation treatments, the original cellulose I crystal structure was maintained. Crystallinity index was slightly decreased from 0.45 to 0.44 and 0.41 by the alkali and methylation treatments, respectively. Probably, DMSO swelled a part of cellulose and TEMPO-oxidized cellulose molecules during the methylation treatment.

Crystal width of the (2 0 0) plane were also somewhat decreased from 3.8 nm to 3.6 nm by these treatments. However, as a whole, the methylation with $TMSCHN_2$ had nearly no influence on the original crystal structure of the fibrous TOC, and the alkali treatment removed 86% of the anhydroglucuronate units present on the TOC microfibril surfaces, without any significant changes in the crystalline cellulose regions present inside TOC nanofibrils.

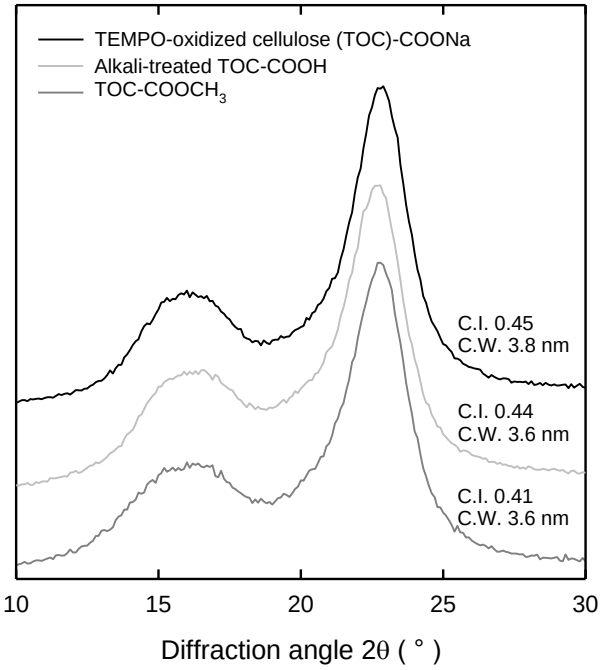

Figure 4.3. X-ray diffraction patterns of TEMPO-oxidized cellulose (TOC) with sodium carboxylate groups of 1.68 mmol g^{-1}, alkali-treated TOC with free carboxyl groups of 0.23 mmol g^{-1} and TOC with methyl ester groups. C.I.= crystallinity index; C.W.= crystal width of (2 0 0) plane.

Figure 4.4 shows FT-IR spectra of the fibrous TOC-COONa, alkali-treated TOC-COOH and carboxyl groups-methylated TOC. The absorption peak at 1603 cm^{-1} due to C=O stretching vibration of sodium carboxylate groups of the TOC mostly disappeared by the alkali treatment, and a small absorption peak due to residual free carboxyl groups was observed at 1732 cm^{-1}. The small and broad peak around 1640 cm^{-1} is due to bending vibration of residual water in the product. This FT-IR result was consistent with that of carboxylate contents before and after the alkali treatment; 86% of

the carboxylate groups present in the fibrous TOC was removed by the alkali treatment. On the other hand, the absorption peak at 1603 cm^{-1} due to sodium carboxylate groups of the TOC completely disappeared by the methylation, and that due to methyl esters appeared in turn at 1738 cm^{-1}. In the FT-IR study, the methylated TOC was soaked in aqueous NaCl solution under neutral conditions to convert the residual free carboxyl groups, if present, to sodium carboxylate groups. Because pK_a values of C6 carboxyl groups of polyuronic acids are approximately 3.6,[34,35] some free carboxyl groups in the methylated TOC, if present, should be converted to sodium carboxylate groups. However, the FT-IR spectra revealed that almost all carboxyl groups of the fibrous TOC were converted to methyl esters by the $TMSCHN_2$ treatment. No other significant differences in FT-IR patterns were observed before and after these treatments.

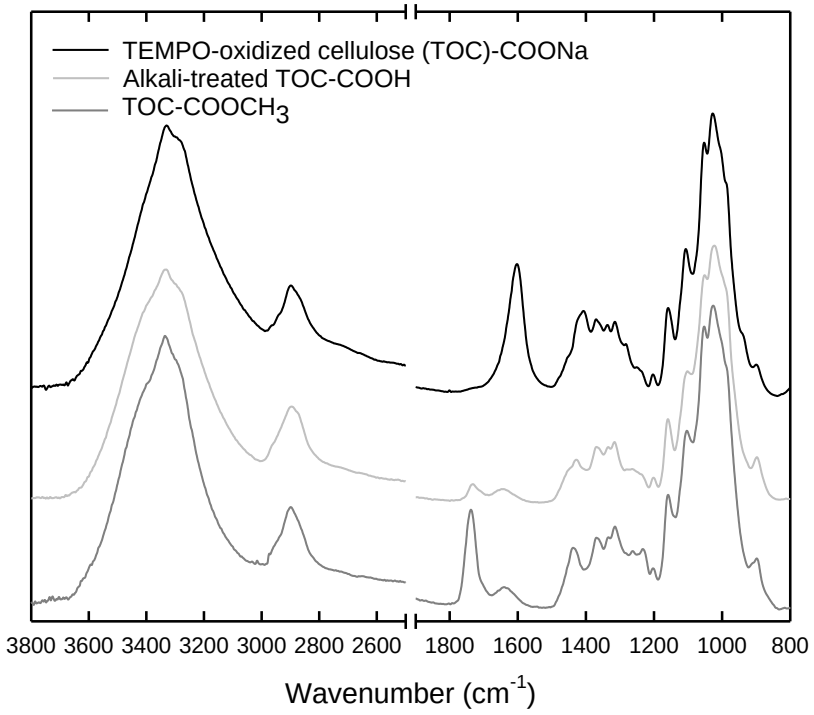

Figure 4.4. FT-IR spectra of TEMPO-oxidized cellulose (TOC) with sodium carboxylate groups of 1.68 mmol g^{-1}, alkali-treated TOC with free carboxyl groups of 0.23 mmol g^{-1} and TOC with methyl ester groups.

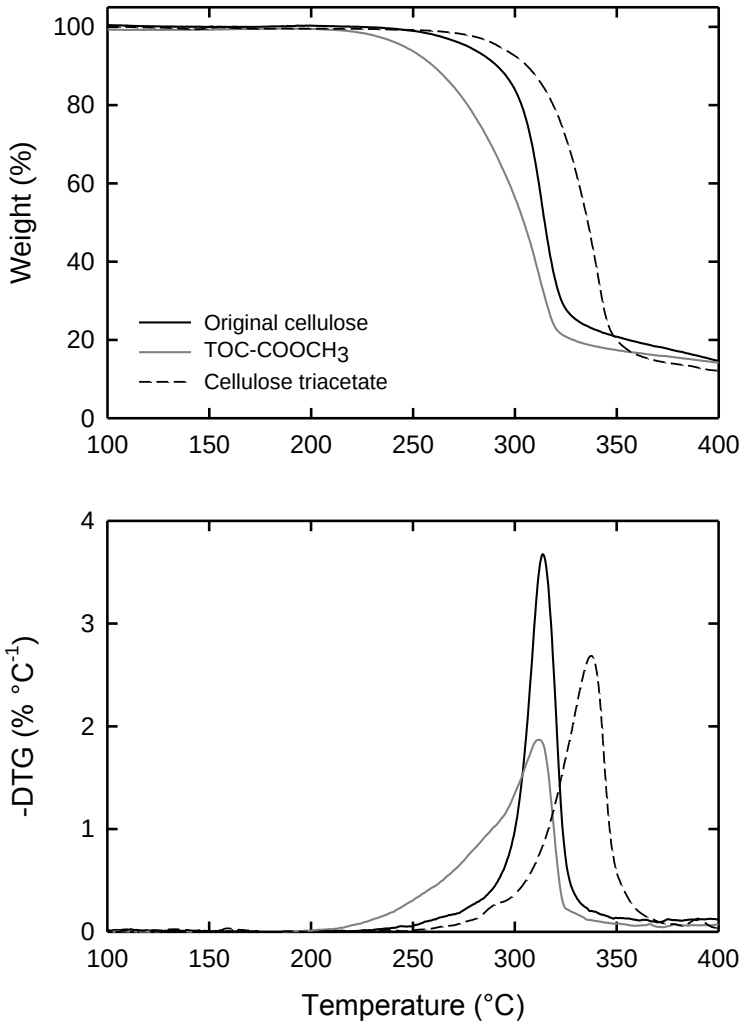

Figure 4.5. Thermogravimetric (upper) and the corresponding derivative thermogravimetric (DTG) (lower) curves of the original cellulose, TEMPO-oxidized cellulose (TOC) with methyl ester groups and cellulose triacetate.

TG and the corresponding DTG curves of the methylated TOC together with those of the original cellulose and cellulose triacetate are drawn in upper and lower graphs, respectively, in Figure 4.5. Methyl esterification of the fibrous TOC-COONa improved its thermal stability from T_d points of 222 ºC to 249 ºC, although this T_d point was still lower than that of the original cellulose (275 ºC). The DTG_{peak} of the methylated TOC was 313 ºC, which was almost equal to that of the original cellulose (314 ºC). Thus, thermal stability of the TOC was significantly improved by methylation of carboxyl

groups, although the methylated TOC had a much broader peak pattern than that of the original cellulose. The thermal stabilization of TOC by methyl esterification may caused by a similar function of thermally-stable cellulose acetate.[9] However, the methylated TOC was not thermally stable as the original cellulose (Figure 4.5). Conceivably, unhomogeneous chemical structure of TOC and/or methylated TOC may influence on their T_d behavior.

4.3.3 The effect of counter ion-exchange treatments

As shown in the previous sections, carboxyl groups of the fibrous TOC strongly influenced its T_d behavior, and methylation of carboxyl groups was effective to improve thermal stability. In this section, thermal degradation behavior of the fibrous TOC was further studied by exchanging sodium ions of carboxylate groups to other metal ions. Decarboxylation of sodium carboxylate groups of the fibrous TOC during heating process was expectedly suppressed to some extent by blocking carboxyl groups with other metal ions[17–23] in analogy with the methyl ester blocking described in the previous section.

As depicted in the upper graph of Figure 4.6, potassium, magnesium, calcium, strontium, silver, iron, aluminum and lanthanum ions were introduced to the fibrous TOC as counter ions of carboxylate groups. The metal contents of the counter ion-exchanged TOC samples and pH values of the cellulose slurries varied depending on the metals salts used. The metal contents were relatively high when pH of the cellulose slurries was neutral or weak alkali. The potassium and calcium contents were almost equal to the carboxylate content of the fibrous TOC, when KCl and $Ca(OAc)_2$ solutions were used in the soaking treatments. Thus, the TOC-COOK and TOC-COOCaCl structures were formed in these cases by the ion-exchanging treatments. On the other hand, when KI, $CaCl_2$, $Ca(NO_3)_2$, CaI_2 and $AgNO_3$ solutions were used, the metal ion contents were approximately 2/3 of the carboxylate content of the TOC. When the pH of the cellulose slurry was lower or more acidic, more amounts of free carboxyl groups might be formed in the ion-exchanged TOC sample.

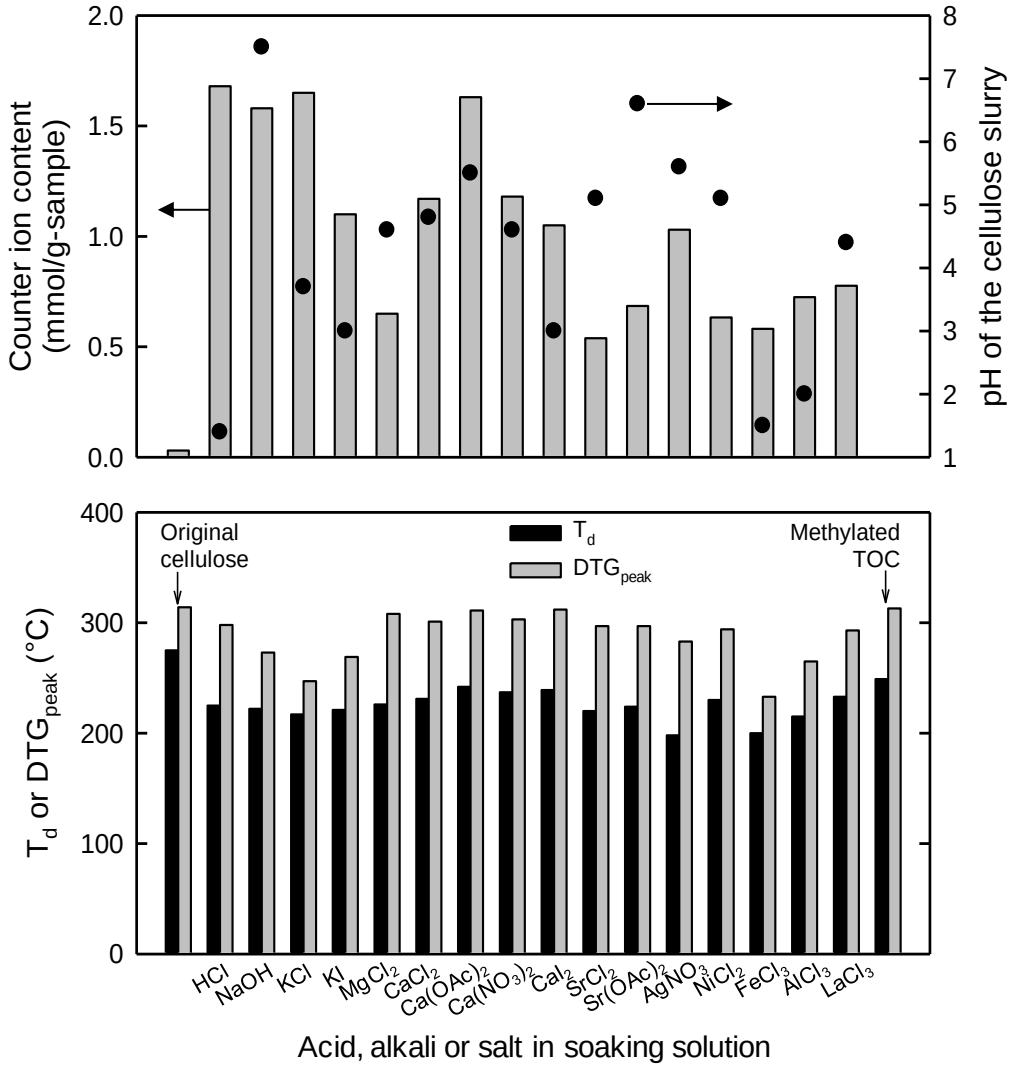

Figure 4.6. Thermal decomposition (T_d) and derivative thermogravimetric peak (DTG_{peak}) temperatures of the original cellulose, TEMPO-oxidized cellulose (TOC)-COOH, TOC-COONa, TOC with methyl ester groups and the TOC samples with various metal carboxylate groups prepared by soaking in salt solutions (lower graph). The upper graph shows the corresponding counter ion contents in the TOC samples and pH values of the cellulose slurries.

Divalent or trivalent metal ions can form the salt structure like cross-linking with two or three carboxyl groups of TOC, resulting in the lower counter ion contents. In fact, $FeCl_3$, $AlCl_3$ and $LaCl_3$ in the soaking solutions were prone to give the metal ion contents relatively lower than those for monovalent and divalent metal ions.

Furthermore, some metal ion contents obtained in this study for TEMPO-oxidized softwood kraft pulps were somewhat different from those reported in the previous paper for TEMPO-oxidized cotton linters with carboxylate content of 0.48 mmol g^{-1}, even when the same metal salts were used.[6] Probably, difference in carboxyl contents and/or slight differences in the ion-exchange treatment conditions such as stirring rates, solid contents, washing procedures with water and others between the present and previous studies might delicately influence the resultant metal ion contents.

The T_d and DTG_{peak} temperatures of the counter ion-exchanged TOC samples as well as the original cellulose, TOC-COOH, TOC-COONa and TOC-$COOCH_3$ are displayed in the lower graph in Figure 4.6. These results show that formation of some metal carboxylate groups can improve thermal stability of the fibrous TOC to some extent, depending on the metal ions introduced. When thermal stability was evaluated as T_d points, the ion-exchange treatments with $Ca(OAc)_2$, CaI_2, $Ca(NO_3)_2$, $LaCl_3$ and $CaCl_2$ solutions gave 242–231 ºC, which were higher than the T_d point of the fibrous TOC-COONa (222 ºC). However, the improved levels were lower than for the methyl esterification. On the other hand, the $AgNO_3$ and $FeCl_3$ solutions gave T_d points lower than that of the TOC-COONa. The effect of these metal ions on T_d behavior of cellulosic materials were reported elsewhere.[12,22] Detailed mechanisms for the positive or negative improvement of thermal stability for the TOC by the counter ion-exchange treatments are unknown at present. This is because the differences in T_d points between the samples were not so remarkable, and the moles of metal ions introduced varied. However, it was prone that introduction of calcium counter ions in place of sodium ions into the fibrous TOC improved thermal stability to some extent.

On the other hand, when thermal stability was evaluated by DTG_{peak}, the $MgCl_2$, $CaCl_2$, $Ca(OAc)_2$, $Ca(NO_3)_2$ and CaI_2 solutions gave the peak temperatures of 312–301 ºC, which were close to those of the original cellulose and methylated TOC (313 ºC). Thus, these divalent metal ions are effective to improve thermal stability of the fibrous TOC. However, again the detailed mechanisms for these results have not been explainable. It was not necessarily the case that the greater the ionic radius of the metal

ion introduced, the higher the DTG_{peak} temperature.[22] Hence, the ion-exchange treatments with some salt solutions can improve thermal stability of the TOC to some extent, although the improved levels are lower than methyl esterification of carboxyl groups.

4.3.4 Modifications of carboxyl groups to improve thermal stability

As described in the above sections, thermal stability of the TOC can be improved to some extent by methyl esterification or counter ion-exchange treatments of carboxyl groups in the TOC. However, these methylated and counter ion-exchanged TOC fibers are unlikely to maintain the original nanofibrillation behavior of the TOC-COONa fibers, when disintegrated in water. Thus, these modifications of carboxyl groups may be applicable to TOC fibers for improvement of their thermal stability. Moreover, it is also plausible that the modifications of carboxyl groups are applied to once-cast TOC nanofibril films for improvement of their thermal stability. However, in the next stage, it should be made clear whether or not the characteristic properties of the TOC-nanofibril films with sodium carboxylate structures such as extremely low oxygen-permeability values, high light-transparencies, low thermal expansion coefficients and high strengths are observed at similar levels also for the carboxyl groups-modified TOC nanofibril films with higher thermal stability.

4.4 Conclusions

A partially C6-carboxylated cellulose with carboxylate content of 1.68 mmol g^{-1} was prepared by 2,2,6,6-tetramethylpiperidinyl-1-oxyl radical (TEMPO)-mediated oxidation of softwood bleached kraft pulps. Thermogravimetric analyses of the TEMPO-oxidized cellulose (TOC) and its related materials were studied to improve thermal stability of the TOC. Thermal decomposition (T_d) points of the TOC with sodium carboxylate groups, alkali-treated TOC with free carboxyl groups of 0.23 mmol g^{-1} and the original cellulose were 222 ºC, 264 ºC and 275 ºC, respectively. Thus, the anhydroglucuronic

acid units formed by TEMPO-mediated oxidation of the native wood cellulose and present in the TOC cause the decrease in T_d by decarboxylation during heating process. When carboxyl groups in the TOC were methylated with trimethylsilyl diazomethane ($TMSCHN_2$), the T_d point increased from 222 ºC to 249 ºC, and the peak temperature in its derivative thermogravimetric (DTG) curve increased from 273 ºC to 313 ºC, which was almost equal to that of the original cellulose. Thus, the methyl esterification of carboxyl groups in the TOC is effective in improving thermal stability. When sodium ions present in the TOC as counter ions of carboxylate groups were exchanged to some other metal ions, thermal stability was improved to some extent. Especially, when $CaCl_2$, $Ca(OAc)_2$, $Ca(NO_3)_2$ and CaI_2 solutions were used in the ion-exchange treatments, the peak temperatures in the DTG curves increased to approximately 300 ºC. $MgCl_2$, $NiCl_2$, $SrCl_2$ and $Sr(OAc)_2$ solutions were also effective to some extent in increasing the peak temperatures of DTG curves. Thus, thermal stability of the fibrous TOC can be improved to some extent by methyl esterification of the sodium carboxylate groups present in the original TOC with $TMSCHN_2$ or ion-exchange treatments with some metal salt solutions.

References

1. Hashimoto, N.; Aoyama, T.; Shioiri, T. *Chem. Pharm. Bull.*, **1981**, 29, 1475–1478.
2. Presser, A.; Hüfner, A. *Monatsh. Chem.*, **2004**, 135, 1015–1022.
3. Ciucanu, I.; Kerek, F. *Carbohydr. Res.*, **1984**, 131, 209–217.
4. Kühnel, E.; Laffan, D. D. P.; Lloyd-Jones, G. C.; Martinez del Campo, T.; Shepperson, I. R.; Slaughter, J. L. *Angew. Chem. Int. Ed.*, **2007**, 46, 7075–7078.
5. Tot, I.; Müller, Y.; Werner, C.; Rosenau, T.; Potthast, A. *Holzforschung*, **2009**, 63, 657–663.
6. Saito, T.; Isogai, A.; *Carbohydr. Polym.*, **2005**, 61, 183–190.
7. Klarman, A. F.; Galanti, A. V.; Sperling, L. H. *J. Polym. Sci. A-2*, **1969**, 7,

1513–1523.

8. Kamide, K.; Saito, M.; *Polym. J.*, **1985**, 17, 919–928.
9. Huang, M. R.; Li, X. G.; *J. Appl. Polym. Sci.*, **1998**, 68, 293–304.
10. Williams, P. T.; Horne, P. A. *Renewable Energy*, **1994**, 4, 1–13.
11. Nik-Azar, M.; Hajaligol, M. R.;. Sohrabi, M.; Dabir, B. *Fuel Process. Technol.*, **1997**, 51, 7–17.
12. Richards, G. N.; Zheng, G. *J. Anal. Appl. Pyrolysis*, **1991**, 21, 133–146.
13. Hanna, A. A.; Basta, A. H.; El-Saied, H.; Abadir, I. F. *Polym. Degrad. Stab.*, **1999**, 63, 293–296.
14. Müller-Hagedorn, M.; Bockhorn, H.; Krebs, L.; Müller, U. *J. Anal. Appl. Pyrolysis*, **2003**, 68–69, 231–249.
15. Davies, P. H.; Horrockes, A. R.; Anderson, A. *Polym. Degrad. Stab.*, **2005**, 88, 114–122.
16. Shimada, N.; Kawamoto, H.; Saka, S. *J. Anal. Appl. Pyrolysis*, **2008**, 81, 80–87.
17. Parks, E. J.; Hebert, R. L. *Tappi J.*, **1972**, 55, 1510–1514.
18. Kaushik, R. K.; Gur, I. S.; Bhatnagar, H. L. *Thermochim. Acta.*, **1989**, 145, 331–352.
19. Tian, C. M.; Xie, J. X.; Guo, H. Z.; Xu, J. Z. *J. Therm. Anal. Calorim.*, **2003**, 73, 827–834.
20. Kleen, M.; Gellerstedt, G. *J. Anal. Appl. Pyrolysis*, **1995**, 35, 15–41.
21. Patwardhan, P. R.; Satrio, J. A.; Brown, R. C.; Shanks, B. H. *Bioresour. Technol.*, **2010**, 101, 4646–4655.
22. Britto, D.; Assis, O. B. G. *Thermochim. Acta.*, **2009**, 494, 115–122.
23. Jakab, E.; Mészáros, E.; Borsa, J. *J. Anal. Appl. Pyrolysis*, **2010**, 87, 117–123.
24. Okita, Y.; Saito, T.; Isogai, A. *Biomacromolecules*, **2010**, 11, 1696−1700.
25. Soares, S.; Camino, G.; Levchik, S. *Polym. Degrad. Stab.*, **1995**, 49, 275−283.
26. Antal, M. J. J.; Varhegyi, G. *Ind. Eng. Chem. Res.*, **1995**, 34, 703–717.
27. Lin, Y.-C.; Cho, J.; Tompsett, G. A.; Westmoreland, P. R.; Huber, G. W. *J. Phys. Chem. C*, **2009**, 113, 20097–20107.

28. Saito, T.; Isogai, A. *Biomacromolecules*, **2004**, 5, 1983–1989.
29. Isogai, T.; Yanagisawa, M.; Isogai, A. *Cellulose*, **2009**, 16, 117–127.
30. Szcześniak, L.; Rachocki, A.; Tritt-Goc, J. *Cellulose*, **2008**, 15, 445–451.
31. Raemy, A.; Schweizer, T. F. *J. Thermal. Anal.*, **1983**, 28, 95–108.
32. Waymack, B. E.; Belote, J. L.; Baliga, V. L.; Hajaligol, M. R. *Fuel*, **2004**, 83, 1505–1518.
33. Perlin, A. S. *Can. J. Chem.*, **1952**, 30, 278–290.
34. Hirota, M.; Tamura, N.; Saito, T.; Isogai, A. *Carbohydr. Polym.*, **2009**, 78, 330–335.
35. Tamura, N.; Hirota, M.; Saito, T.; Isogai, A. *Carbohydr. Polym.*, **2010**, 81, 592–598.

CHAPTER 5

Influence of nanofibril length on film properties of TEMPO-oxidized cellulose nanofibril

5.1 Introduction

The self-standing TOCN films and TOCN-coated films have been studied in terms of optical, mechanical, thermal and gas-barrier properties in the previous chapters. It has been reported that optical and mechanical properties of nano-sized cellulose sheets are influenced by degrees of polymerization (DP), crystallinities and chemical compositions of celluloses used.[1] In the case of TOCNs, their fibril lengths (and fibril length distributions as well) should have somewhat influences on optical, mechanical and gas-barrier properties. Even though TOCNs prepared from wood celluloses have almost homogeneous widths of 3–4 nm, their lengths and length distributions vary, depending on the preparation conditions of TOCNs. However, the influence of TOCN lengths on the film properties has not been studied in detail. The fibril lengths of TOCNs are controllable by controlling the pH of the TEMPO-mediated oxidation system[2] or the amount of NaClO added in the TEMPO-mediated oxidation in water at pH 10).[3] In these cases, however, remarkable changes in carboxylate contents of TOCNs are unavoidable, and thus the influence of TOCN fibril length alone on TOCN film properties cannot be extracted from the obtained results.

In this chapter, therefore, we first prepared a TEMPO-oxidized wood cellulose with a carboxylate content of 1.5 mmol g^{-1}, and various mechanical disintegration conditions were applied to the TEMPO-oxidized cellulose in water to prepare TOCNs with different nanofibril lengths. Self-standing TOCN films and TOCN-coated plastic films were prepared, and their optical, mechanical and gas-barrier properties were evaluated in terms of the nanofibril length.

5.2 Experimental section

5.2.1 Materials

A never-dried softwood bleached kraft pulp was used as the cellulose source for TEMPO-mediated oxidation. The pulp had a viscosity average DP (DP_v) of 1200, when 0.5M copper ethylene diamine (cuen) was used as the solvent.[4] The pulp contained approximately 90% cellulose and 10% hemicelluloses. Laboratory grade TEMPO, sodium bromide, and 13% sodium hypochlorite solution (Wako Pure Chemicals, Co. Ltd., Japan) were used as received. TEMPO-oxidized cellulose was prepared from the softwood cellulose using the TEMPO/NaBr/NaClO system at pH 10 according to the procedure written in experimental section 2.2.1. The TEMPO-oxidized cellulose thus prepared had a DP_v of 550 and a sodium carboxylate content of 1.5 mmol g^{-1}. Commercial poly(ethylene terephthalate) (PET) films (Teijin DuPont Films, Japan), and poly(lactic acid) (PLA) films (Mitsui Chemical Tohcello, Inc., Japan) were used as coating substrates.

5.2.2 Preparation of TOCN water dispersions

An aqueous 0.15% slurry of the TEMPO-oxidized cellulose was subjected to blender-type homogenization at 15000 rpm (Excel Auto ED-4, Nissei, Japan) for 5 or 10 min, and subsequently sonicated at 19.5 kHz and 300 W output power (26 mm probe tip diameter, US-300T, Nissei, Japan) for 2, 4 or 20 min (Table 5.1). Three transparent aqueous dispersions (TOCN-a, -b, and -c) were obtained after centrifugation of the dispersions at 12000 g for 10 min to remove unfibrillated and partly fibrillated fractions. The yields of TOCNs after centrifugation are described in Table 5.1.

Table 5.1. Preparation conditions and properties of TOCNs.

	Homogenization time (min)	Sonication time (min)	Nanofibril yield (%)	Average nanofibril length (nm)	DPv [a]
TOCN-a	10	20	ca. 100	200	250
TOCN-b	10	4	98	680	350
TOCN-c	5	2	85	1100	400

[a] Viscosity-average degree of polymerization determined using 0.5M cuen as the solvent.

5.2.3 Preparation of TOCN films

Self-standing wood TOCN films ~10 μm in thickness were prepared by pouring the TOCN dispersions in poly(styrene) petri dishes and drying at 40 °C for 3 days. The TOCN films were easily detached from the dish after drying. TOCN-coated films ~1.5 μm in TOCN thickness were prepared as follows. The PET films (thickness 50 μm; area 9 × 9 cm^2) and PLA films (thickness 25 μm; area 9 × 9 cm^2) were surface-hydrophilized by plasma exposure at 5 mA for 5 min in vacuum using a soft-etching device (DSDE-AF, Meiwafosis Co., Ltd., Japan). The 0.15% TOCN/water dispersion (10 ml) was uniformly cast onto the hydrophilized surface of the base film and allowed to natural drying at room temperature for 3 days.

5.2.4 Analysis

DP values of TOCNs were measured by the following method. Freeze-dried TOCNs (0.5 g) were reacted with sodium chlorite (0.1 mmol) in an acetate buffer (50 mL) at pH 4.5 and room temperature for 2 day to selectively oxidize small amounts of C6-aldehydes to C6-carboxylates.[5] After all carboxyl groups were converted to sodium carboxylate groups with a diluted NaOH solution, the $NaClO_2$-oxidized TOCNs were purified and isolated by dialysis against water and subsequent freeze-drying. The freeze-dried samples thus obtained (0.04 g) were dissolved in 0.5 M cuen, and their viscosities were measured using a capillary viscometer. The DP_v values of the $NaClO_2$-oxidized TOCNs were calculated from their intrinsic viscosities.[4]

Samples for TEM observation were prepared as follows. A 10 μl aliquot of 0.015% (w/v) TOCN dispersions was mounted on a glow-discharged carbon-coated electron microscopy grid, and the excess liquid was absorbed by a filter paper. One drop of 1% uranyl acetate negative stain was added before drying, and the excess solution was also wiped with a filter paper. The stained TOCN dispersions were allowed to natural evaporation until drying. The sample grids were observed at 200 kV using a JEOL electron microscope (JEM 2000-EX).

The self-standing TOCN films were conditioned in desiccators at designed relative

humidities for at least 48 h, and measured their weights at a resolution of ± 2 μg. Dry weights of the films were measured after drying the films at 105 °C for 3 h followed by storing them in desiccators with P_2O_5 for 3 h. Water contents of the self-standing TOCN films at various relative humidities under equilibrium conditions were gravimetrically calculated from the conditioned and dried weights.

Fourier transform infrared (FT-IR) spectra of the self-standing TOCN films were recorded using a Jasco FT/IR-6100 spectrometer under transmission mode from 400 to 4000 cm^{-1} with 4 cm^{-1} resolution. Crystallinity indices of cellulose I for the TOCN films were calculated from the IR spectra by the absorption ratios, A_{cryst} at 1372 cm^{-1}/A_{total} at 2900 cm^{-1}.[6,7]

Light transmittance spectra of the TOCN/water dispersions and dried TOCN films were measured from 200 to 1000 nm with a Shimadzu UV-vis-NIR spectrophotometer (Jasco, V-670, Japan). Film thicknesses of self-standing TOCN films and TOCN layers on the coated films were calculated by using the JASCO's analysis program from the interference pattern which appeared in transmittance and/or reflectance spectra according to a reported method.[8] In order to measure film thickness, refractive index of the target substance must be given. The refractive indices 1.55, 1.65, and 1.49 were used for TOCN, PET and PLA, respectively.[9,10]

Tensile tests of self-standing TOCN films with ~15 μm thickness were carried out at 23 °C and 50% relative humidity (R.H.) using a Shimadzu EZ-TEST tensile tester equipped with a 500 N load cell. Specimens with at least 20 mm length and 2 mm width were measured at 1.0 mm min^{-1} and 10 mm span length, and at least 5 specimens were measured for each sample.

The PET and PLA films coated with TOCNs were subjected to oxygen permeability rate (OTR) determination at 23 °C and various relative humidities using an oxygen permeability testing apparatus (Mocon OX-TRAN 2/21, Modern Controls Inc., U.S.A.) according to a standard method (ASTM 3985). Each sample was conditioned in a desiccator at a designed R.H. for at least 12 h before the measurement. The test areas were 50 cm^2 and 5 cm^2 for films with low and high OTRs, respectively. Each sample

was conditioned in a chamber of the OTR system for 3 h, and the OTR was measured for more than 1 day until it reached a stable value. Water vapor transmission rates (WVTR) of the films were measured using a Mocon PERMATRAN-W 1/50 according to a standard method (ASTM 398). The cell in detector side was set at 10% R.H., and the other side was varied from 40 to 100% R.H. The WVTR value was measured for more than 1 h until it reached a stable value.

5.3 Results and discussion

5.3.1 Nanofibril lengths and length distributions of TOCNs

The 0.15% w/v TOCN/water dispersions were visually transparent, and the apparent viscosities were in the order of TOCN-c >TOCN-b >TOCN-a. TEM images of the TOCNs showed that the nanofibrils were clearly different in length depending on the mechanical disintegration conditions, while they had almost uniform widths of 4 nm (Figure 5.1). More than 200 nanofibrils for each TOCN sample were used to measure lengths and length distributions using an image-J software. Even if some kinks were present in each nanofibril, they were ignored for the length calculation. The length distribution histograms were asymmetrical, and extended toward the longer part in a similar manner for cellulose nanowhiskers.[11] The length-weighted average lengths were 200 nm, 680 nm and 1100 nm for TOCN-a, -b, and -c, respectively. Thus, the length of TOCN is controllable by selecting the mechanical disintegration conditions of the TOCN/water slurry, keeping the same fibril widths. The TOCN-a had lengths ranging from 50 to 750 nm, while TOCN-b had those from 120 to 2100 nm. TOCN-c had a much wide length distribution from 110 to 3600 nm. Sharp blades of the blender-type homogenizer would mechanically cut the nanofibrils in various ranges.

Mechanical disintegration times and properties of three TOCNs are listed in Table 5.1. Because almost complete individualization was achieved for TOCN-a, the nanofibril yield was almost 100%. In the case of TOCN-c, the nanofibril yield decreased to 85%, because it contained a larger amount of unfibrillated and partly fibrillated

fraction due to short disintegration times. The DP_v values of TOCNs also decreased with decreasing the average nanofibril length, showing that TOCN lengths are correlated to their DP_v values; the TOCN lengths become shorter in association with depolymerization.

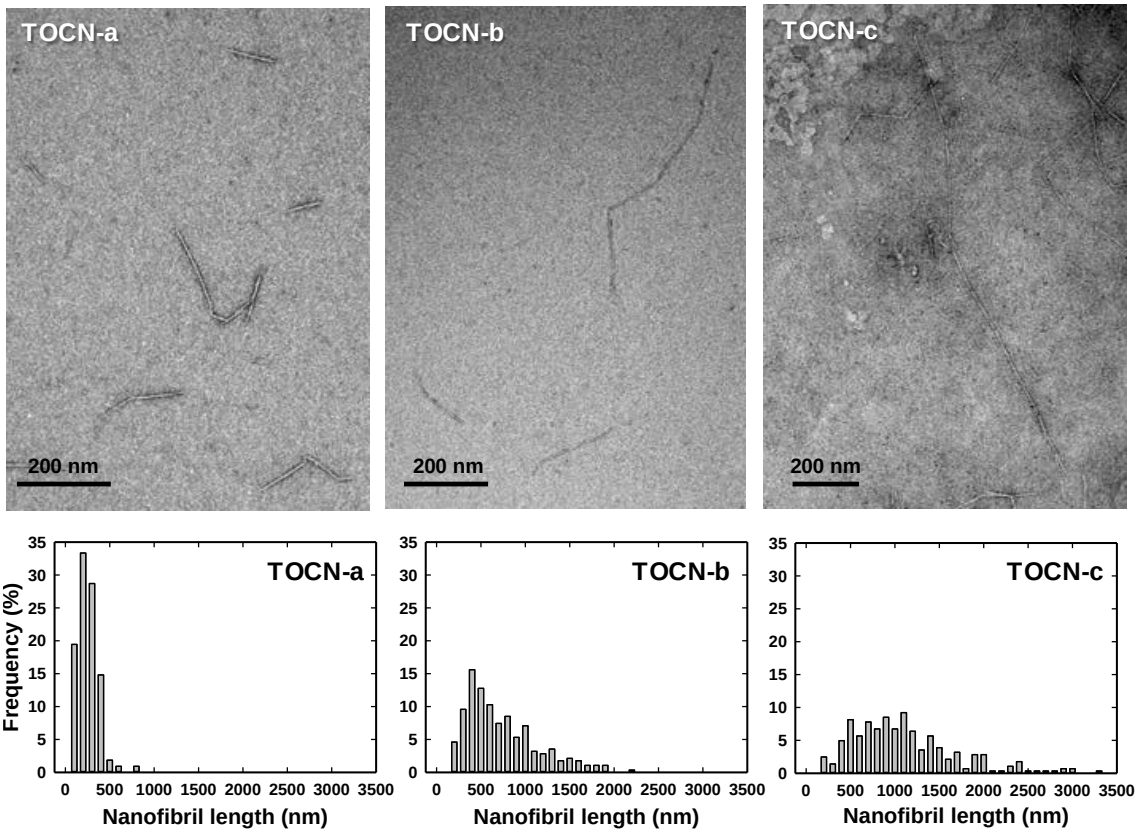

Figure 5.1. TEM images of TOCN-a, TOCN-b, and TOCN-c, and their length distributions measured on the corresponding TEM images.

5.3.2 Optical and mechanical properties of TOCN films

Light transmittances of self-standing TOCN films 10 μm in thickness are shown in Figure 5.2. All TOCN films had light transmittances of >80% at 600 nm, which are in good agreement with those in the section 2.3.2 (Figure 2.2). The interference at the near-infrared region indicates high smoothness of the film surfaces and uniformity of the film thickness in large surface areas.[12] The films prepared from TOCN-a had a slightly higher light transmittance than the others. Short nanofilbrils of TOCN-a prepared by long mechanical disintegration times may have, in turn, led to high

dispersibility in water, resulting in low light scattering behavior than for TOCN-b or TOCN-c with longer nanofibrils (Figure 5.3). Thus, the light transmittance or dispersibility of TOCN in water, shown in Figure 5.3, reflects the transparency of the self-sanding TOCN films in Figure 5.2.

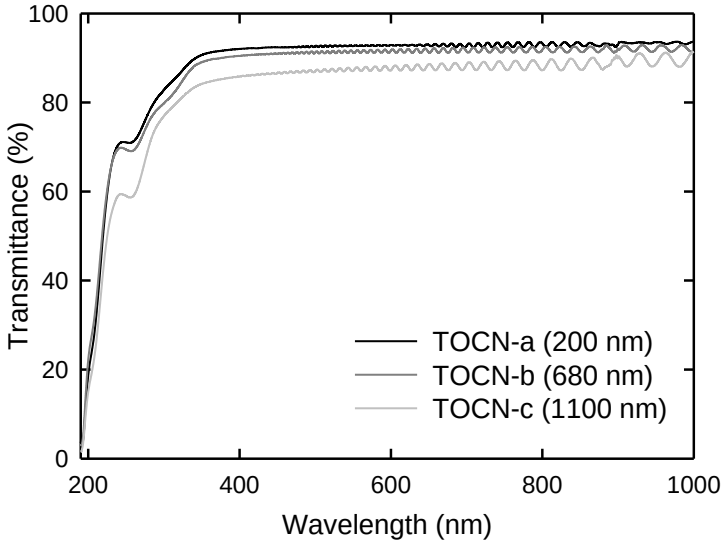

Figure 5.2. UV-vis light transmittance spectra of self-standing TOCN films with 10 μm thickness.

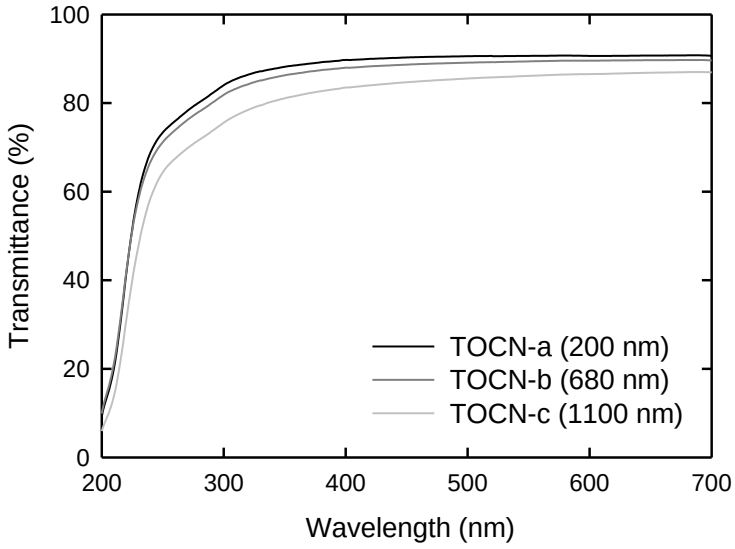

Figure 5.3. UV-vis light transmittance spectra of 0.15% TOCN/water dispersions.

Typical stress-strain curves of the self-standing TOCN films are shown in Figure 5.4. In particular, the tensile strength increased with increasing nanofibril length from TOCN-a to TOCN-c in association with the increased elongation at break. The film densities, water contents at 23 °C and 50% R.H., elastic moduli, tensile strengths, elongation at breaks, and crystallinity indices of the three TOCN films are listed in Table 2. These three TOCN films had quite similar densities of about 1.4 g cm^{-3} and water contents of ~12%, showing that the TOCN films have similar hygroscopic and dense structures. Meanwhile, the TOCN films had higher tensile strength and greater elongation at break as the average nanofibril length and DP_v were increased; these properties are strongly influenced by the nanofibril length and length distributions.

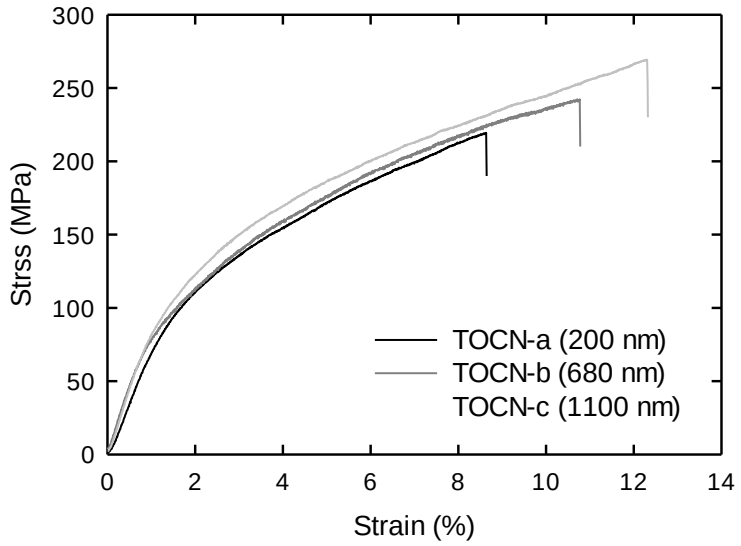

Figure 5.4. Stress-strain curves of TOCN films during tensile test.

Table 5.2. Properties of self-standing TOCN films. Density and water content of the films were measured at 23 ºC and 50% R.H.

	Density (g/cm^3)	Water content (%)	Elastic modulus (GPa)	Tensile strength (MPa)	Elongation at break (%)	Crystallinity index [a]
TOCN-a (200 nm)	1.40	12.2	8.8 ± 1.4	224 ± 25	8.9 ± 0.9	0.56
TOCN-b (680 nm)	1.42	12.3	9.4 ± 0.7	257 ± 22	9.0 ± 1.3	0.59
TOCN-c (1100 nm)	1.43	11.6	9.8 ± 0.8	266 ± 10	9.9 ± 1.6	0.64

[a] Calculated from each IR spectrum by the absorption ratio, $A_{1372\ cm\text{-}1}/A_{2900\ cm\text{-}1}$.[6]

The higher elastic moduli of the TOCN-b and TOCN-c films may be sensitively reflected by the slightly higher film densities (Table 5.2).[1,13] Elastic moduli of the TOCN films may also be correlated to their crystallinity indices.[13,14] IR crystallinity indices of cellulose I for the self-standing TOCN films (Table 5.2) were determined from FT-IR spectra according to the reported method (Figure 5.5).[6] The IR crystallinity index increased with increasing the nanofibril length, indicating that the higher elastic modulus and density and lower water content of the TOCN-c films are probably due to higher crystallinity index of cellulose I. The amount of disordered both edge parts of nanofibrils may increase with decreasing the nanofibril length by longer times of mechanical disintegration of the TEMPO-oxidized cellulose in water. Tensile strength and elongation at break of TOCN films substantially increased with the nanofibril length. It was reported that increased DP caused higher elongation at breaks associated with higher tensile strengths.[1]

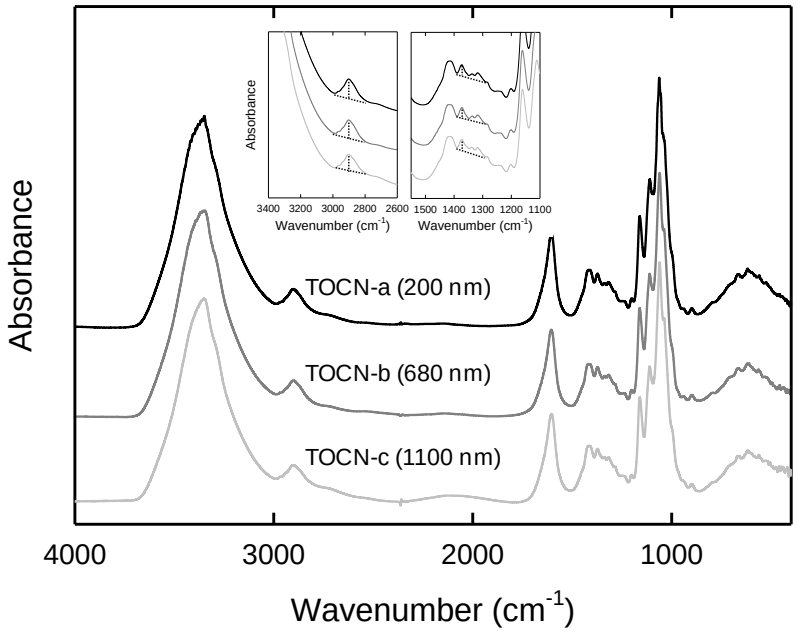

Figure 5.5. FT-IR spectra of self-standing TOCN films. The inserts show the expanded FT-IR spectra of self-standing TEMPO-oxidized cellulose nanofibril (TOCN) films for calculation of their crystallinity indices of cellulose I. Each crystallinity index is calculated from the absorption ratio, A_{cryst} at 1372 cm^{-1}/A_{total} at 2900 cm^{-1}.[6]

5.3.3 Oxygen and water vapor permeability of TOCN films

Oxygen transmission rates (OTRs) of the TOCN-coated PET and PLA films under various R.H. values are depicted in Figure 5.6. OTRs of the base films were almost unchanged in the whole R.H. range due to their hydrophobic nature; PET and PLA base films had high OTRs of ~30 and ~900 mL m^{-2} day^{-1} kPa^{-1}, respectively. To the contrary, oxygen permeability of hydrophilic TOCN-coated films was strongly influenced by R.H. OTRs of TOCN-coated PET and PLA films were extremely low at 0% R.H., while they exponentially increased with increasing R.H. The OTR values at 35% R.H. increased approximately two orders of magnitude of that at 0% R.H., and they became close to the OTRs of the base films at 75% R.H. In the three TOCNs, TOCN-c showed the highest oxygen-barrier properties in the 0–50% R.H. range. The difference between the three TOCNs clearly appeared at 0% R.H., and became less at 75% R.H. Because the self-standing TOCN-c film had the highest crystallinity index, the high crystallinity of cellulose I in the TOCN-c-coated films may have caused the high oxygen-barrier properties. In addition, the pore sizes in the TOCN layers may have become smaller as the nanofibril length becomes longer (and length distribution becomes wider as well). A similar result was reported, when oxygen permeability was compared between microfibrillated cellulose and cellulose nanowhisker films with longer and shorter nanocellulose lengths, respectively.[15]

On the contrary, the nanofibril length had almost no influence on the water vapor transmission rates (WVTRs) of the TOCN-coated films (Figure 5.7). The WVTR increased linearly with increasing R.H. The increasing patterns of WVTRs with R.H. were similar to that of the base film, but the WVTR values of the TOCN-coated films were lower than that of the base film at the same R.H. This is probably due to increased thickness of the TOCN-coated films. Figure 5.8 shows relationships between R.H. and water content of the self-standing TOCN films under equilibrium conditions. No significant differences in water content at each R.H. were observed between the three TOCN films, showing that the amounts of adsorbed water in the TOCN films at each

R.H. are quite similar regardless of the nanofibril length. Although the self-standing TOCN films had high water vapor permeability of approximately 70 g μm m^{-2} day^{-1} kPa^{-1} at 30% R.H and this value exponentially increased with increasing R.H. (See Figure 2.7 in Chapter 2), the WVTRs could be suppressed to low values in the whole R.H. range as shown in Figure 5.7 by coating TOCNs on hydrophobic PET or PLA films; the hydrophilic nature of TOCNs is controllable by coating TOCNs on hydrophobic base polymer films to have low OTRs and WVTRs even under high R.H. conditions.

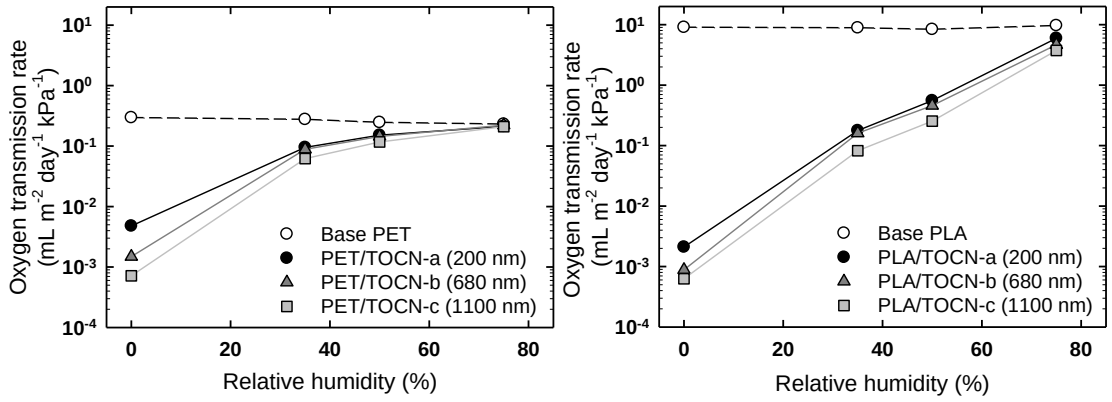

Figure 5.6. Oxygen transmission rates of TOCN-coated PET (left) and PLA (right) films. Thicknesses of the PET and PLA base films were 50 μm and 25 μm, respectively. TOCN layers with approximately 1.5 μm thickness were coated on the base films.

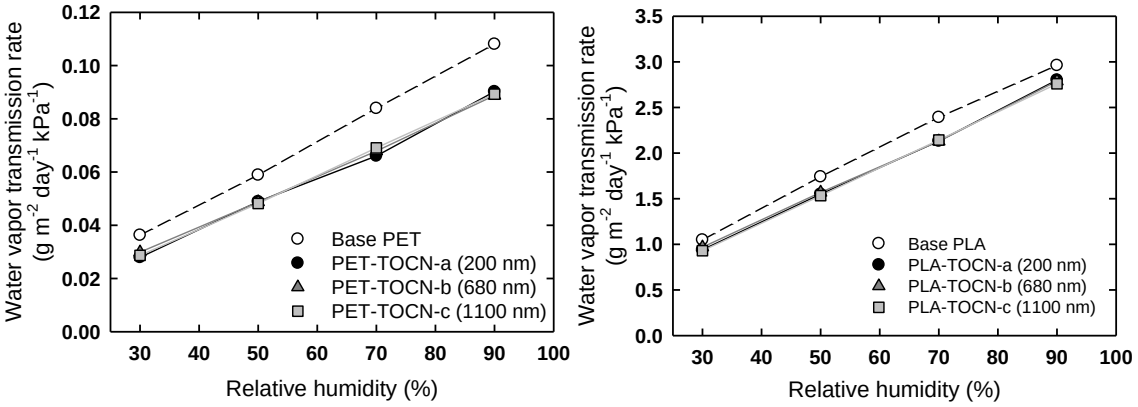

Figure 5.7. Water vapor transmission rates of TOCN-coated PET (left) and PLA (right) films. See Figure 5.6 for details of the base films and coating layers.

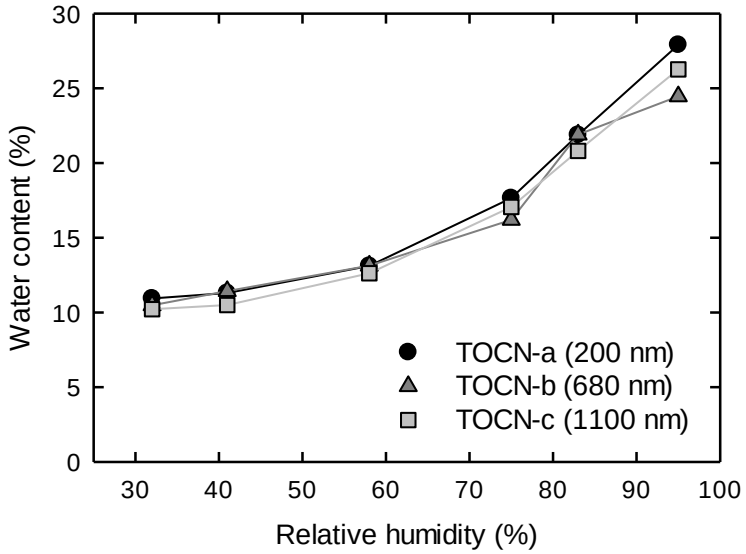

Figure 5.8. Water contents of TOCN films at 23 °C and various relative humidities under equilibrium conditions.

5.4 Conclusion

The influence of TOCN length on optical, mechanical, and gas-barrier properties of TOCN films was investigated using TOCNs with three different nanofibril lengths. The shorter the average TOCN length, the lower the DP_v of TOCN and the higher the light transmittances of both the TOCN/water dispersion and the TOCN film. The differences in density and water content at 23 °C and 50% R.H. were small between the three self-standing TOCN films prepared from TOCNs with three different nanofibril lengths. On the contrary, the longer the average TOCN length, the higher the tensile strength and elongation at break of the TOCN films. Oxygen-barrier properties between the three TOCN-coated films were different particularly at low R.H.; the longer the nanofibril length, the higher the oxygen-barrier properties. On the contrary, nanofibril length of TOCNs had almost no influence on water vapor barrier properties, which were primarily influenced by the water vapor transmission rates of the hydrophobic base films.

References

1. Henriksson, M.; Berglund, L. A.; Isaksson, P.; Lindström, T. *Biomacromolecules*, **2008**, 9, 1579–1585.
2. Saito, T.; Hirota, M.; Tamura, N.; Kimura, S.; Fukuzumi, H.; Heux, L.; Isogai, A. *Biomacromolecules,* **2009**, 10, 1992–1996.
3. Shinoda, R.; Saito, T.; Okita, Y.; Isogai, A. *Biomacromolecules*, in press.
4. Shitola, H.; Kyrklund, B.; Laamanen, L.; Palenlus, I. *Pap. Puu*, **1963**, 45, 225–232.
5. Saito, T.; Isogai, A. *Biomacromolecules*, **2004**, 5, 1893–1989.
6. Nelson, M. L.; O'coonor, E. T. *J. Appl. Polym. Sci.*, **1964**, 8, 1325-1341.
7. Okita, Y.; Fujisawa, S.; Saito, T.; Isogai, A. *Biomacromolecules*, **2011**, 12, 518–522.
8. Lin, K.; Chen, Y. *J. Sol-Gel Sci. Technol.*, **2009**, 51, 215–221.
9. Isogai, A.; Saito, T.; Fukuzumi, H. *Nanoscale*, **2010**, 3, 71–85.
10. Auras, R.; Harte, B.; Selke, S. *Macromol. Biosci.*, **2004**, 4, 835–864.
11. Elazzouzi-Hafraoui, S.; Nishiyama, Y.; Putaux, J. L.; Heux, L.; Dubreuil, F.; Rochas, C. *Biomacromolecules*, 2008, 9, 57–65.
12. Takahashi, M.; Iyoda, K.; Miyauchi, T.; Ohkido, S.; Tahashi, M.; Wakita, K.; Kajitani, N.; Kurachi, M.; Hotta, K. (2009). Preparation and characterization of Eu: Ti codoped LiNbO3 films prepared by the sol-gel method. *J. Appl. Phys.*, **2009**, 106, 044102.
13. Retegi, A.; Gabilondo, N.; Peña, C.; Zuluaga, R.; Castro, C.; Gañan, P.; la Caba, K.; Mondragon, I. *Cellulose*, **2010**, 17, 661–669.
14. Iwamoto, S.; Nakagaito, A. N.; Yano, H. (2007). *Appl. Phys. A*, **2007**, 89, 461–466.
15. Belbekhouche, S.; Bras, J.; Siqueira, G.; Chappey, C.; Lebrun, L.; Khelifi, B.; Marais, S.; Dufresne, A. *Carbohyd. Polym.*, **2011**, 83, 1740–1748

CHAPTER 6

Summary

6.1 Preparation and structure of TEMPO-oxidized cellulose nanofibril film

TEMPO-mediated oxidation and subsequent mechanical homogenization were applied to mainly softwood bleached kraft pulp to prepare TEMPO-oxidized cellulose nanofibrils (TOCNs). The prepared TOCNs had almost uniform width of 3–4 nm and length over 200 nm. The nanofibril length can vary by mechanical homogenization conditions. When the average TOCN length is shorter, the degree of polymerization of TOCN becomes lower as well. Self-standing film was prepared by filtration of TOCN aqueous dispersions using a membrane with 0.1 μm pore size or casting the dispersion on a petri dish. In both cases, the ambient drying temperature was about 40 ºC. TOCN-coated film was obtained by casting a TOCN aqueous dispersion on plastic films, such as polyethylene terephthalate (PET) and polylactic acid (PLA), and drying them at room temperature. Before coating treatment, the base films had to be hydrophilized beforehand.

Microscopic observations of the TOCN films with sodium carboxylate groups (TOCN-COONa) revealed that the film consists of densely accumulated nanofibril layers in the cross-section, while random orientation of TOCNs were observed for the film surfaces. The dense structure of nanofibrils in the TOCN films resulted in a constant pore size of about 0.47 nm and homogeneous pore distribution from surface to interior of the TOCN film, when measured by positron annihilation lifetime spectroscopy (PALS). The pore size and pore distribution were unchanged by heating treatment at 150 °C for 0.5 h. The densities and moisture contents of the TOCN films were rather similar to those of commercial cellophane.

6.2 Properties of TEMPO-oxidized cellulose nanofibril film

TOCN films with sodium carboxylate groups (TOCN-COONa) showed properties as follows; (1) high visible-light transparency, (2) thermal stability up to 200 ºC, (3) thermal dimensional stability, (4) flexibility & high tensile strength, (5) high oxygen-barrier properties, (6) high water-vapor permeability, and (7) surface hydrophilicity. In addition, reinforcing effect was observed in the composite film of polyvinyl alcohol with TOCNs. The details about each property of TOCN films are listed below.

(1) The transparency was slightly different between softwood and hardwood TOCN films, and between TOCN films with various nanofibril lengths. It was likely to be affected by dispersibility of nanofibrils in water dispersions.

(2) The thermal decomposition temperature of TOCN films significantly decreased from that of the original cellulose probably owing to decarboxylation of anhydroglucuronate units, which were formed by TEMPO-mediated oxidation and presented in TOCNs. When carboxyl groups of the TEMPO-oxidized cellulose were converted to methyl esters with trimethylsilyl diazomethane ($TMSCHN_2$), the thermal decomposition temperatures were clearly increased by about 50 ºC. Additionally, when the sodium carboxylate groups were converted to calcium carboxylate groups by ion-exchange treatments using calcium chloride, calcium acetate, calcium nitrate, and calcium iodide, improvements in thermal stability were also observed to some extent. Therefore, thermal stability of the TOCN films can be improved by methyl esterification or some ion-exchange treatments of the sodium carboxylate groups present in TOCN surfaces.

(3) The thermal expansion coefficient of TOCN films was much lower than that of glass. It was possibly caused by the high crystallinity of the nanofibrils and also rigid network structures comprising the TOCN film.

(4) The tensile properties of TOCN films were slightly different between softwood and hardwood TOCN films, and between TOCN films with varous nanofibril lengths.

The values of elastic modulus, the tensile strength, and the elongation at break of TOCN films do correlate with nanofibril lengths and length distributions. The longer nanofibrils with large length distribution resulted in higher values of the three mechanical parameters. Tensile properties of the TOCN films may be more related to their densities than dispersibility of nanofibrils in water.

(5) The oxygen-barrier property of TOCN films was extremely high at dry condition because of the small pore size of the film and the crystalline structures of TOCN. However, this property degraded with increasing relative humidity of the measurement atmosphere owing to hydrophilic nature of TOCNs. This drawback may be overcome by coating TOCN on hydrophobic substrates. Nanofibril length and length distribution were significantly influenced on this property. The longer nanofibrils with large length distribution resulted in better oxygen-barrier property when measured even at high relative humidity.

(6) The water-vapor permeability of TOCN films was affected by not only hydrophilic nature of cellulose, but also sodium carboxylate groups present on the TOCN surface. TOCN film with sodium carboxylate groups (TOCN-COONa) adsorbed much water than for the TOCN film with free carboxyl groups (TOCN-COOH). Water-vapor transmission rates of TOCN-coated films were as much as those of hydrophobic base films (PET and PLA). The hydrophilic nature of TOCN can be controllable by some hybridization with hydrophobic films.

(7) The surface hydrophilicity of TOCN films was observed as low contact angles of water on the TOCN film. It was as low as that of cellophane, and decreased with time. This affected by both hydrophilic nature of cellulose and sodium carboxylate groups on the TOCN surface. Surface hydrophobization was achieved by a simple soaking treatment in an alkylketene dimer (AKD) dispersion or addition of small amount of AKD into a TOCN aqueous dispersion. The water-contact angle of TOCN film treated with AKD was around 100°, and no penetration of water was observed at least for 10 s.

ACKNOWLEDGEMENT

This thesis is a compilation of studies carried out from April 2006 to March 2011 under the supervision of Professor Akira Isogai in the University of Tokyo. During the six years, I received Bachelor and Master degrees in Biomaterial Sciences from the University of Tokyo in 2007 and 2009, respectively. I would like to express my deepest respect and gratitude to Professor Akira Isogai for his warm encouragement and considerate guidance throughout this study.

I am grateful to Associate Professor Toshiharu Enomae for his continuous encouragement and advice throughout this study. I am greatly indebted to Assistant Professor Tsuguyuki Saito for his instructions and suggestions. He has been care for my research from the beginning by teaching me the preparation method of cellulose nanofibrils, many analytical techniques, and writing techniques of scientific papers. I would like to thank Assistant Prof. Minoru Kimura for his encouragement and valuable advice to this study. Thanks are also due to my friends and colleagues; Dr. Hirotaka Koga and Mr. Takehiko Uematsu for many valuable discussions concerning this study, Mr. Yusuke Kurita and Mr. Naoyuki Tamura for the helps of NMR analysis, Mr. Syuji Fujisawa for the helps of FT-IR analysis, and all the other members in the Paper Science Laboratory for their kind cooperation and advice.

I would like to acknowledge the following former colleagues who kindly supported my experiments and had valuable discussions. Assistant Professor Daisuke Ishi of Ryukoku University, Japan. Dr. Yoshiaki Kumamoto, Dr. Yutaka Yoshida and Mr. Kenta Mukai of Kao Corporation, Japan. Dr. Yota Mori of Tokushu Tokai Paper Co., Ltd., Japan. Dr. Shinichiro Iwamoto of National Institute of Advanced Industrial Science and Technology, Japan. Associate Professor Yimin Fan of Nanjing Forestry University, China. Dr. Takuya Isogai of Toppan Printing Co., Ltd., Japan. Dr. Yusuke Okita of Unitika Ltd., Japan.

Special thanks to Assistant Professor Satoshi Kimura and Mr. Noriyuki Isobe for their support in SEM observation; Associate Professor Akio Takemura and Associate Professor Tadahisa Iwata for their insightful advice in mechanical analysis; and Associate Professor Yukie Saito for her guidance in thermogravimetry.

I would like to express my gratitude to Dr. Ryoichi Suzuki and Dr. Toshiyuki Ohdaira of National Institute of Advanced Industrial Science and Technology for the enormous contribution to PALS analysis.

I am grateful to Professor Takeshi Kikutani of Tokyo Institute of Technology, Japan for his constructive comments on film structure; Assistant Professor Masaya Nogi of Institute of Science and Industrial Research, Osaka University, Japan for his advice and warm encouragement to this study; Professor Olli Ikkala of Ålto University, Finland for his constructive comments on gas permeability of the cellulose nanofibril film.

I sincerely thank my family for their devoted support and encouragement.

The financial support was provided by the Japan Society for the Promotion of Science (JSPS), Grants-in-Aid for Scientific Research (grant number 21-6112) from 2009 to 2011.

Finally, I would like to thank again Professor Akira Isogai, Professor Takeshi Kikutani, Associate Professor Akio Takemura, Associate Professor Toshiharu Enomae, and Associate Professor Tadahisa Iwata for their devotion to judgment of this PhD thesis.

Hayaka Fukuzumi

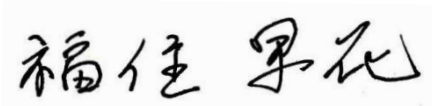

RESEARCH ACHIEVEMENT

PUBLICATIONS

1. Hayaka Fukuzumi, Tsuguyuki Saito, Tadahisa Iwata, Yoshiaki Kumamoto, and Akira Isogai, "Transparent and High Gas Barrier Films of Cellulose Nanofibers Prepared by TEMPO-Mediated Oxidation", *Biomacromolecules*, ACS publications, Vol. 10, No. 1, pp. 162–165 (2009).

2. Hayaka Fukuzumi, Tsuguyuki Saito, Yusuke Okita, and Akira Isogai, "Thermal Stabilization of TEMPO-oxidized Cellulose", *Polymer Degradation and Stability*, Elsevier, Vol. 95, No. 9, pp. 1502–1508 (2010).

3. Hayaka Fukuzumi, Tsuguyuki Saito, Shinichiro Iwamoto, Yoshiaki Kumamoto, Toshiyuki Ohdaira, Ryoichi Suzuki, and Akira Isogai, "Pore Size Determination of TEMPO-Oxidized Cellulose Nanofibril Films by Positron Annihilation Lifetime Spectroscopy", *Biomacromolecules*, ACS publications, Vol. 12, No. 11, pp. 4057–4062 (2011).

4. Hayaka Fukuzumi, Tsuguyuki Saito, and Akira Isogai, "Influence of nanofibril length on film properties of TEMPO-oxidized cellulose nanofibril", *Carbohydrate Polymers*, Elsevier. (To be submitted)

5. Tsuguyuki Saito, Masayuki Hirota, Naoyuki Tamura, Satoshi Kimura, Hayaka Fukuzumi, Laurent Heux, and Akira Isogai, "Individualization of Nano-Sized Plant Cellulose Fibrils by Direct Surface Carboxylation Using TEMPO Catalyst under Neutral Conditions", *Biomacromolecules*, ACS publications, Vol. 10, No. 7, pp. 1992–1996 (2009).

6. Akira Isogai, Tsuguyuki Saito, and Hayaka Fukuzumi, "TEMPO-oxidized cellulose nanofibers", *Nanoscale*, RSC Publishing, Vol. 3, pp. 71–85 (2011).

7. Shuji Fujisawa, Yusuke Okita, Hayaka Fukuzumi, Tsuguyuki Saito, and Akira Isogai, “Preparation and Characterization of TEMPO-oxidized Cellulose Nanofibril Flms with Free Carboxyl Groups”, *Carbohydrate Polymers*, Elsevier, Vol. 84, No. 1, pp. 579–583 (2011).

8. Quanling Yang, Hayaka Fukuzumi, Tsuguyuki Saito, Akira Isogai, and Lina Zhang, “High Gas Barrier and Transparent Cellulose Films Fabricated from Aqueous Alkali-Urea Solution”, *Biomacromolecules*, ACS publications, Vol. 12, No. 7, pp. 2766–2771 (2011).

9. Yimin Fan, Hayaka Fukuzumi, Tsuguyuki Saito, and Akira Isogai, “Comparative Characterization of Aqueous Dispersions and Cast Films of Different Chitin Nanowhiskers/Nanofibers” *International Journal of Biological Macromolecules*, Elsevier, in press (2011). [DOI:10.1016/j.ijbiomac.2011.09.026]

10. 磯貝明、齋藤継之、福住早花「TEMPO 酸化セルロースナノファイバーの調製と機能材料への展開」、未来材料、Vol. 11, No. 10, pp. 33–39 (2011).

PRESENTATIONS

International conference

1. Hayaka Fukuzumi, Tsuguyuki Saito, and Akira Isogai, “Nanofiber films prepared by TEMPO-mediated oxidation of Native Cellulose”, 2nd International Cellulose Conference ICC2007, Tokyo, Japan, October, 2007. [Poster]

2. Hayaka Fukuzumi, Tsuguyuki Saito, and Akira Isogai, “Properties of TEMPO-oxidized cellulose nanofiber film”, 237th ACS National Meeting & Exposition, CELL-204, Salt Lake City, USA, March, 2009. [Oral]

3. Hayaka Fukuzumi, Tsuguyuki Saito, and Akira Isogai, “Influence of nanofiber length on mechanical and gas barrier properties in TEMPO-oxidized cellulose nanofiber films”, 2nd International Polysaccharide Conference (EPNOE 2011), Wageningen, The Netherlands, August, 2011. [Oral]

Conference in Japan

1. 福住早花、磯貝明　「セルロースナノファイバー分散液からのフィルム調製とその特性解析」、セルロース学会　第 14 回年次大会、P14、静岡、2007 年 7 月 [Poster]
2. 福住早花、斉藤継之、磯貝明　「TEMPO 触媒酸化により得られるセルロースナノファイバーフィルム」、第 57 回　日本木材学会大会、K08-1115、広島、2007 年 8 月 [Oral]
3. 福住早花、斎藤継之、磯貝明　「セルロースナノファイバーフィルムの調製および基礎特性」、繊維学会　平成 20 年度次大会、2B01、東京、2008 年 6 月 [Oral]
4. 福住早花、斉藤継之、Fan Yimin、磯貝明　「起源の異なるセルロース、キチンナノファイバーフィルムの特性解析」、セルロース学会　第 15 回年次大会、P52、京都、2008 年 7 月 [Poster]
5. 福住早花、齋藤継之、磯貝明　「TEMPO 触媒酸化により得られるセルロースナノファイバーの基礎特性と複合材料化」、繊維学会　平成 21 年度年次大会、2C10、東京、2009 年 6 月 [Oral]
6. 福住早花、斎藤継之、磯貝明　「透明でガスバリア性を備えた新規セルロースナノファイバーフィルム」、日本包装学会　第 18 回年次大会、P-18、東京、2009 年 7 月 [Poster]
7. 福住早花、齋藤継之、磯貝明　「TEMPO 酸化セルロースの熱安定性の改善」、繊維学会　平成 22 年度年次大会、2P42、東京、2010 年 6 月 [Poster]

8. 福住早花、斎藤継之、磯貝明　「TEMPO 酸化セルロースナノファイバーのガスバリア性」、日本包装学会　第 19 回年次大会、P-1、東京、2010 年 7 月 [Poster]

9. 福住早花、沖田祐介、齋藤継之、磯貝明　「TEMPO 酸化により調製したセルロースナノファイバー：耐熱性およびガスバリア性に関する検討」、セルロース学会　第 17 回年次大会、K10、徳島、2010 年 7 月 [Oral]

10. 福住早花、沖田祐介、齋藤継之、磯貝明　「TEMPO 酸化セルロースのメチルエステル化および金属イオン交換」、第 59 回　高分子討論会、2Pa121、札幌、2010 年 9 月 [Poster]

11. 福住早花、齋藤継之、青山公洋、片桐清文、磯貝明　「TEMPO 酸化セルロースナノファイバー多層フィルムのガスバリア性」、日本包装学会　第 20 回年次大会、A-7、京都、2011 年 7 月 [Oral]

HONORS AND AWARDS

1. Research Fellowship for Young Scientists, Japan Society for the Promotion of Science –April 2009 to May 2011

2. Dean’s Award of the University of Tokyo, Graduate School of Agricultural & Life Sciences –May 2009

3. Dean’s Award of the University of Tokyo –May 2007

4. Best Poster Prize in the 19th Annual Meeting of the Society of Packaging Science & Technology, Japan –July 2010

5. Best Poster Prize in the 18th Annual Meeting of the Society of Packaging Science & Technology, Japan –July 2009